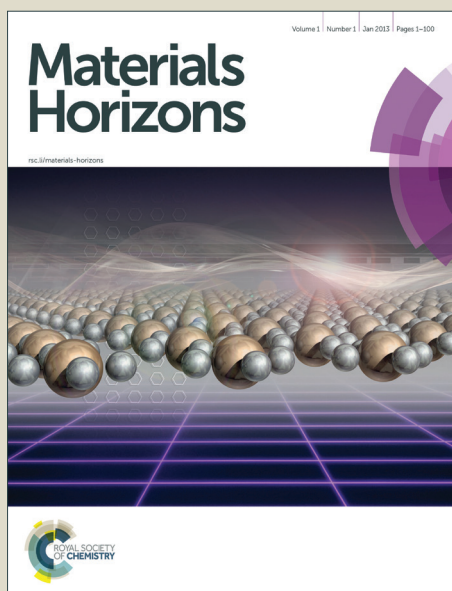


# Materials Horizons

Accepted Manuscript



This is an *Accepted Manuscript*, which has been through the Royal Society of Chemistry peer review process and has been accepted for publication.

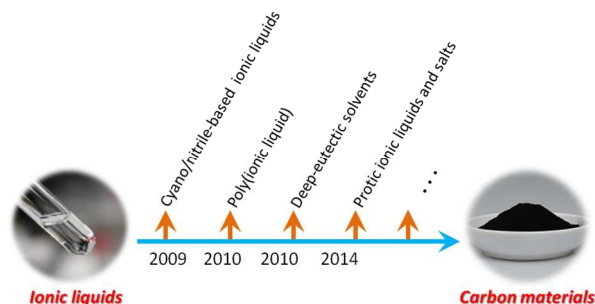
*Accepted Manuscripts* are published online shortly after acceptance, before technical editing, formatting and proof reading. Using this free service, authors can make their results available to the community, in citable form, before we publish the edited article. We will replace this *Accepted Manuscript* with the edited and formatted *Advance Article* as soon as it is available.

You can find more information about *Accepted Manuscripts* in the [Information for Authors](#).

Please note that technical editing may introduce minor changes to the text and/or graphics, which may alter content. The journal's standard [Terms & Conditions](#) and the [Ethical guidelines](#) still apply. In no event shall the Royal Society of Chemistry be held responsible for any errors or omissions in this *Accepted Manuscript* or any consequences arising from the use of any information it contains.

## Carbon Materialization of Ionic Liquids: From Solvents to Materials

Shiguo Zhang, Kaoru Dokko, and Masayoshi Watanabe\*



Synthesis, characteristics, porous design, and potential applications of novel carbon materials derived from ionic liquids precursors have been reviewed, including future trends and prospects in this direction.

## ARTICLE

# Carbon Materialization of Ionic Liquids: From Solvents to Materials

Cite this: DOI: 10.1039/x0xx00000x

Shiguo Zhang, Kaoru Dokko, and Masayoshi Watanabe\*

Received 00th January 2012,  
Accepted 00th January 2012

DOI: 10.1039/x0xx00000x

[www.rsc.org/](http://www.rsc.org/)

Carbon materials have been extensively used in diverse areas, especially in energy-related applications. Traditionally, these materials have been synthesized by carbonization of low-vapor-pressure natural or synthetic polymers. However, the polymer-related procedures are multistep and time consuming because of limited solubility and complicated synthesis. Recently, ionic liquids (ILs), composed of entirely cations and anions, have emerged as a new family of carbon precursors. The carbon-rich nature of ILs, coupled with their attractive properties such as diverse cation–anion combinations, low volatilities, and high thermal stabilities, not only greatly simplifies the entire carbonization process, but also gives rise to carbons with attractive features, which are distinct from those of carbons obtained using conventional polymer precursors, such as very high nitrogen contents and conductivities. In this review, we highlight recent approaches to the preparation of carbon materials using ILs as versatile precursors. We begin with a brief introduction to these novel precursors, discussing the key structures and properties of ILs that enable successful carbonization, and then address synthetic techniques for the fabrication of advanced porous carbons from ILs by either self- or external-template methods, followed by a review of the potential applications of ionic-liquid-derived carbons. The review concludes with an overview of possible directions for future research in this field.

## 1. Introduction

Ionic liquids (ILs) have been a source of interest to scientists and engineers for many decades.<sup>1–4</sup> In particular, the unusual combination of a wide liquid range, substrate–reactant solubility, ionic conductivity, low volatility, and high electrochemical and thermal stabilities has led to an explosion in their use as green, ionic, solvents for a host of processes linked to green chemistry and clean

technology, and as ideal electrolytes for a number of energy-related applications such as batteries,<sup>5</sup> fuel cells,<sup>6</sup> supercapacitors,<sup>7</sup> and dye-sensitized solar cells.<sup>1, 2</sup> In contrast, the use of ILs in materials design and synthesis remains less explored, although several novel applications of IL-based fluids and materials as thermal, magnetic, and optical fluids,<sup>8–10</sup> lubricants,<sup>11</sup> and propellants<sup>12</sup> have been receiving more attention in recent years (Figure 1).<sup>3, 4</sup>



**Shiguo Zhang** received his Bachelor's degree in Chemistry from Hunan Normal University in 2004. He received his PhD degree in 2010 in Physical Chemistry from the Lanzhou Institute of Chemical Physics (LICP), Chinese Academy of Sciences (CAS), and worked as an assistant researcher in the LICP from 2010 to 2012. In April 2012, he joined the group of Prof. Masayoshi Watanabe as a postdoctoral at the Yokohama

National University. His research interests focus on design and synthesis of nanostructured carbon materials and their applications in energy conversion and storage.



**Kaoru Dokko** is an Associate Professor of Yokohama National University. He received Ph.D. degree from Tohoku University in 2001 under the supervision of Prof. Isamu Uchida. He then did his postdoctoral research at Case Western Reserve University with Prof. Daniel A. Scherson and at Tokyo Metropolitan University with Prof. Kiyoshi Kanamura, and joined Yokohama National University in 2008. His current research

interests are the physicochemical properties of concentrated electrolytes, nanostructured materials for energy conversion and storage, and electrochemical reaction process in electrochemical devices.

In contrast, because of their high surface areas, electrical conductivities, low costs, and excellent chemical, mechanical, and thermal stabilities, carbon materials have been extensively used in diverse areas such as environmental treatment, catalysis, sensing, separation, gas capture/storage, and, particularly, as electrode materials or electrocatalysts for energy conversion/storage.<sup>13-18</sup> Carbon materials are generally prepared by carbonization of carbon-containing precursors at high temperature. The nature of the organic precursor is crucial to the preparation process (*e.g.*, interactions between precursor and template<sup>19</sup>), and the structures, properties, and performances of the final carbons. The chemical compositions of the precursors are often reflected in the final carbons, and strongly affect characteristics such as the carbon yield, porosity, surface area, graphitization, conductivity, and heteroatom doping. Most organic compounds are completely evaporated or decomposed to gaseous products during high-temperature carbonization, therefore currently available precursors are rather limited, and are mainly low-vapor-pressure natural or synthetic polymers.<sup>20</sup> However, polymer-related procedures are multistep and time consuming. Moreover, for carbons derived from “hard carbon” precursors such as sucrose and furfuryl alcohol, the graphitic structure and nitrogen content, which account for high conductivity, are always insufficient for task-specific applications.<sup>20</sup> To meet the requirements of most applications, great efforts have therefore been devoted to the development of novel precursors.

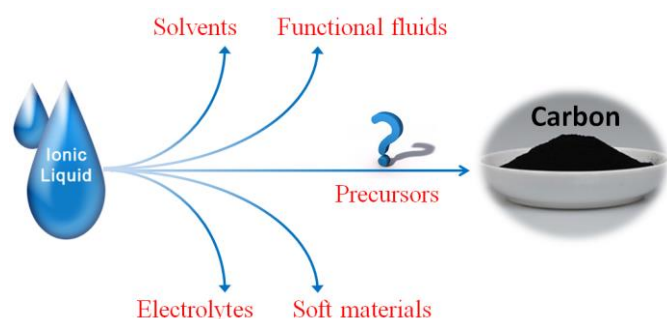


**Figure 1** Ionic liquids as novel precursors for carbon materials.

Let us return to ILs. The cation–anion combinations of ILs, coupled with their carbon-rich natures, make them potential candidates as carbonaceous precursors with the following merits. (a) The intrinsic ionic nature and strong coulombic interactions between the constituent ions give rise to negligible vapor pressure and high thermal stability; these reduce mass loss before the beginning of the decomposition process and are favorable for carbonization processes without applied pressure. (b) Carbonization of small-molecular precursors is easy to handle compared with polymers, which have limited solubility

and require complicated syntheses, simplifying the overall carbonization process, and reducing the preparation time and cost. (c) The nitrogen-containing motifs of ILs incorporate carbons with homogeneously distributed nitrogens *in situ*, without any doping agents. (d) The liquid state under ambient conditions facilitates the production of seamless continuous carbon films. (e) The interactions between the polar IL precursor and the polar surfaces of inorganic materials may assist successful fabrication of advanced carbon materials such as hollow porous carbon or nitrogen-doped carbon-coated materials. (f) The structural diversity offers additional possibilities for easily controlling the structures and properties of the final carbon.<sup>21,22</sup>

Based on an analysis of the previous literature, including the most recent articles, the present review is an attempt to highlight recent progress in the development of IL-based carbon precursors. This review is divided into the following sections. First, we will briefly introduce the recent development in the synthesis of carbon materials from ILs, and the IL-based precursors will be roughly classified into five types, *i.e.*, Cyano/nitrile-containing ILs, conventional aprotic ILs, poly(ionic liquid)s (poly-ILs), deep-eutectic solvents (DESS), and protic ILs (PILs) and protic salts (PSs); these are then discussed separately. For each class, the structural and physicochemical correlations between the original precursors and resultant carbon, if available, will be concisely reviewed, in terms of the carbonization mechanism and characteristics of the carbon such as carbon yield, conductivity, heteroatom doping, and graphitic structure. Secondly, the use of ILs as surface-coating agents and dopants, and as media for the synthesis of carbon materials will be reviewed. Thirdly, synthesis of metal-doped carbons from ILs will be discussed. Fourthly, strategies for the fabrication of porous carbons from ILs such as template-free, nanocasting methods, mainly based on silica and salt templates, will be discussed. Fifthly, the potential applications of IL-derived carbons such as electrocatalysis, supercapacitors, gas adsorption, li-ion batteries (LIBs), and chemical catalysis are demonstrated. Finally, the challenges and prospects for future research on the development of IL-based carbons are discussed.

## 2. Ionic liquids as carbon precursors

### 2.1. Cyano/nitrile-containing ILs

Despite the attractive features of IL-based organic carbon precursors, a question still arises: Can their high thermal stability make ILs sufficiently robust to endure harsh carbonization conditions and ensure carbon yields as substantial



**Masayoshi Watanabe** is a Professor of Yokohama National University. He received his Ph.D. degrees from Waseda University in 1983. After a visiting scientist with Prof. Royce W. Murray at University of North Carolina (1988–1990), he joined Yokohama National University in 1992 and was promoted to a full Professor in 1998. He received the Lecture Award for Young Scientists

from the Chemical Society of Japan in 1991, the Award for Creative Work from the Electrochemical Society of Japan in 2006, the Award of the Society of Polymer Science, Japan in 2006, and Distinguished Research Award of Yokohama National University in 2012. His research interest has been mainly concerned with “ionics” and “nano-structured materials” for chemical energies such as fuel cell and lithium-ion and lithium-sulfur batteries. He has published more than 300 original research papers and 150 books and reviews in these and relating fields; cited more than 14000 times (H-index: 60).

as those obtained using polymer precursors? The answer is “yes”, but the thermal stability and the extent of decomposition depend strongly on the IL structure. In the very early study performed by MacFarlane and coworkers,<sup>23</sup> the thermogravimetric (TG) profiles of dicyanamide ([DCA])- or tricyanomethide ([C(CN)<sub>3</sub>])-based ILs showed that residual yields remained up to 500 °C. This interesting phenomenon was further investigated in detail by Scott *et al.*<sup>24</sup> They found that the extent of decomposition of the IL depends on the structures of both the cation and anion. ILs with nitrogen-containing cations and [DCA] or [C(CN)<sub>3</sub>] anions do not decompose completely to volatile products, yielding an intractable char, but phosphonium-based ILs with [DCA] as the anion, and ILs containing the [NTf<sub>2</sub>] anion, decompose completely to volatile products in a single step, leaving no significant residues. Unfortunately, the obtained chars were not investigated in detail, and the pyrolysis temperature was too low to produce fully carbonized samples.

The first real connection between ILs and carbon materials emerged in 2009, and was developed by Dai *et al.*<sup>25</sup> Through the synergistic use of the negligible vapor pressures of ILs and incorporation of cross-linkable functional groups into the cationic structures, they developed a high-yield and solvent-free route to nitrogen-rich carbons *via* direct, atmospheric-pressure carbonization of task-specific imidazolium ILs bearing one or more nitrile side chains ([MCNIm] and [BCNIm], Figure 2), without any other treatments. Although no carbon yield was achieved from the attempted carbonization of [BMIm][NTf<sub>2</sub>], in agreement with Scott's conclusion,<sup>24</sup> significant yields were observed for all nitrile-functionalized ILs, with the thermal stability depending strongly on the nature of the anion. The resulting textural properties such as pore structure and surface area are highly dependent on the structural motifs of the ions comprising the corresponding parent IL. The carbon yields at 800 °C are very close to the theoretical values, suggesting nearly quantitative transformations of the overall carbon contents of the precursors. Uniform carbon films can be routinely deposited using this novel method, by virtue of the liquid nature.

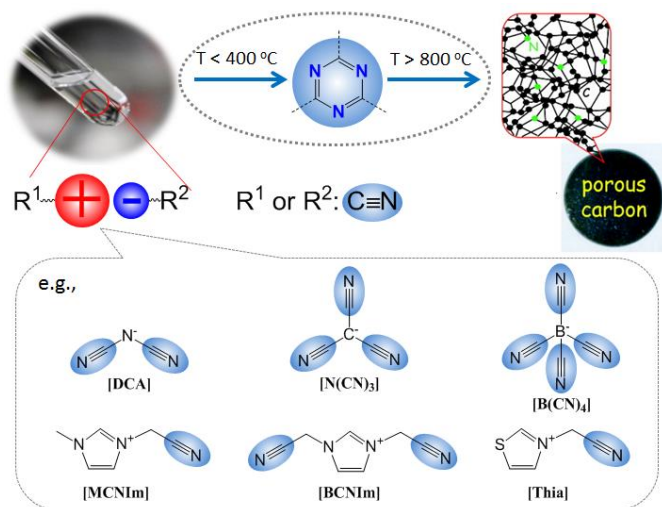


**Figure 2** Direct synthesis of nitrogen-doped carbon from specific nitrile/cyano-containing IL precursors under ambient pressure.

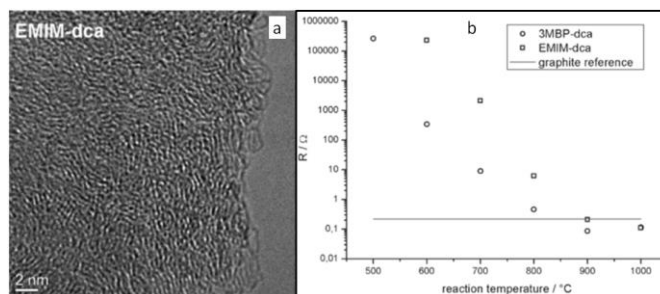


**Figure 3** (a) High-resolution transmission electron microscopy (HRTEM) image of nitrogen-doped carbon material derived from [EMIm][DCA] at 900 °C. (b) Electrical resistances of samples measured using electrical impedance spectroscopy. [Reprinted with permission from Ref. 26, copyright 2010 Wiley.]

Nearly parallel with the work done by Dai *et al.*, Antonietti *et al.* investigated the carbons obtained *via* direct carbonization of [DCA]-anion-based ILs in detail.<sup>26</sup> One distinctive feature of [DCA]-based ILs is their high nitrogen contents; for example, the N/C molar ratio of [EMIm][DCA] (Figure 2) is 0.63 (39.5 wt% N), which is expected to give highly nitrogen-doped carbons. The resultant carbon is indeed featured by a very high nitrogen content, up to 10.4 wt% at 1000 °C.<sup>26</sup> Combining this IL with natural nitrogen-rich nucleobases for carbonization further improves the nitrogen content to 12.0 wt%; this ultrahigh nitrogen content is the highest value for a one-step synthesis of nitrogen-doped carbon reported to date.<sup>27</sup> This high nitrogen content is important, considering that nitrogen doping in the carbon lattice can significantly alter or improve the physicochemical properties of carbon materials, such as their conductivity, basicity, oxidative stability, and catalytic activity, for potential applications.<sup>28–30</sup> Another important property of carbons derived from [DCA]-based ILs is a partially developed graphite-like structure. As shown in Figure 4, the materials are featured by graphitic order with bent layer planes and weak edge termination; this and their intrinsic high nitrogen content result in high conductivities, even higher than that of graphite (Figure 3).<sup>26</sup> After these pioneering studies, a series of ILs that are structurally close to well-understood IL precursors and are designed so that either the cation or anion contains a cyano/nitrile group (Figure 2) were synthesized and used as carbon precursors.<sup>31–34</sup>

Based on TG-MS analysis,<sup>35</sup> the carbonization of [DCA]-based ILs can be divided into three major steps: at around 300 °C, decomposition is initiated by the cleavage of alkyl chains, elimination of ammonia, and other reactions at the lower-molecular level. This is followed by condensation of the material by trimerization of cyano groups, and aromatic condensation, up to approximately 500 °C. On further increasing the temperature to 1000 °C, the reaction is dominated by condensation of the entire system, with elimination of hydrogen and nitrogen, giving rise to the formation of graphitic domains. The role of cyano functional groups is therefore highly important, permitting the first and essential step of formation of a resin that is preorganized and thermostable. As shown in Figure 2, this reaction proceeds at lower temperatures (ca. 400 °C) *via* the formation of dynamic amorphous polytriazine networks,<sup>36–38</sup> depressing the evaporative loss of intermediate volatile species and ensuring subsequent carbonization at higher temperatures. Based on the intermediate triazine-based charged structure formed during pyrolysis of cyano-containing ILs, a new class of microporous polymers with ion-exchange capabilities was developed by

pyrolysis of specific ILs with bisnitrile-functionalized cations, for the adsorption of perrhenate ions in aqueous solution (Figure 4a).<sup>39</sup> The successful carbonization of ILs based on cross-linking reactions of cyano moieties was further proved by the synthesis of nitrogen-enriched carbons from alkali salts containing  $[\text{C}(\text{CN})_3]$  anions.<sup>40</sup> It should be noted that compared with the cations, which are typically based on an imidazolium backbone, the anions are more easily designed to bear multiple cross-linkable components such as two nitrile groups in [DCA], three nitrile groups in  $[\text{C}(\text{CN})_3]$ , and four nitrile groups in tetracyanoborate ( $[\text{B}(\text{CN})_4]$ ).  $[\text{B}(\text{CN})_4]$ , in particular, is expected to be more favorable for the formation of three-dimensional connected intermediate carbonaceous frameworks (Figure 4).

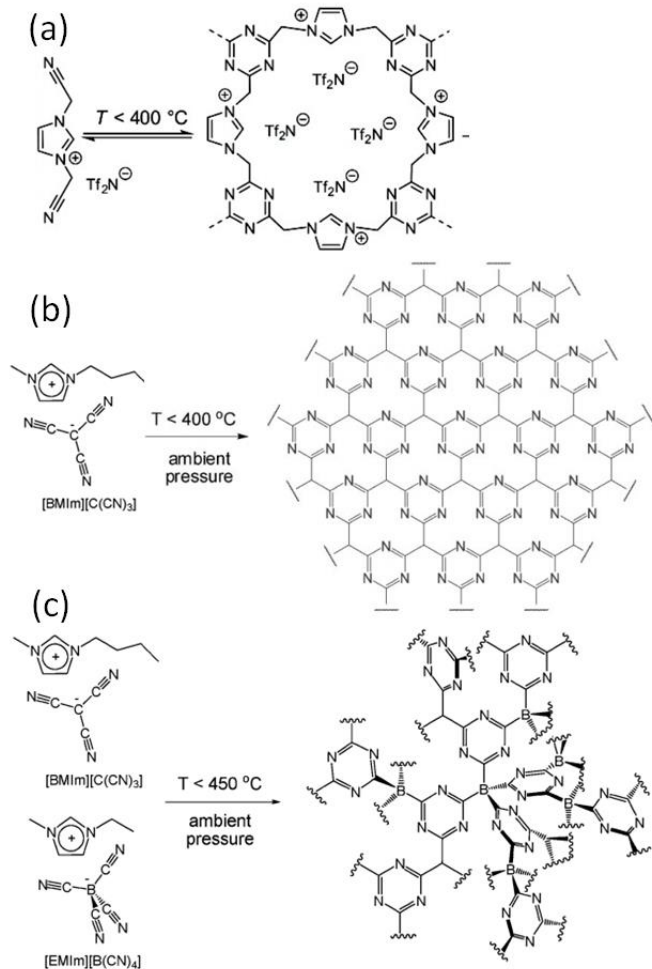


**Figure 4** Proposed reaction scheme for trimerization of nitrile-containing anion, leading to formation of an extended two- or three-dimensional framework. [Panel (a) reprinted with permission from Ref. 25, copyright 2009 American Chemical Society. Panel (b) reprinted with permission from Ref. 31, copyright 2010 Wiley. Panel (c) reproduced from Ref. 41 with permission from the PCCP Owner Societies.]

Multiple doping is a promising method for functionalizing carbon materials. The presence of heteroatoms other than nitrogen, such as boron and sulfur, in the cationic or anionic backbone facilitates synthesis of codoped carbon from ILs.<sup>33, 34, 41-43</sup> For example, an  $[\text{EMIm}][\text{B}(\text{CN})_4]$  IL containing boron,

carbon, and nitrogen was investigated as a direct precursor for the synthesis of boron- and nitrogen-rich carbons or boron carbon nitrides at elevated temperatures.<sup>33</sup>  $[\text{EMIm}][\text{B}(\text{CN})_4]$  decomposes *via* an unusual process, with thermal stability above  $400\text{ }^\circ\text{C}$ , which could be related to the low nucleophilicity and low basicity of the anion. At temperatures above  $1000\text{ }^\circ\text{C}$ , the product starts to become a graphitic boron carbon nitride (BCN) with a weakly ordered structure and a B:N ratio of 1:1. The final material, prepared at  $1400\text{ }^\circ\text{C}$ , has a composition close to  $\text{BC}_3\text{N}$ . In the corresponding reference samples of nitrogen-doped carbon from [DCA]-based ILs, the nitrogen content decreases significantly with increasing temperature, therefore the presence of boron in  $[\text{EMIm}][\text{B}(\text{CN})_4]$  stabilizes the nitrogen within the structure and the BCN units rearrange to a more stable aromatic arrangement. The electrical resistivity in the temperature range  $0\text{--}950\text{ }^\circ\text{C}$  reflects the semiconducting behavior of the BCN, and its electrical resistivity is only 1.75 times less than that of nitrogen-doped carbon.

The presence of sulfur atoms in cations, instead of anions, with nitrile functionalities should alter the carbonization processes in a way that allows the incorporation of not only nitrogen, but also sulfur, into the developing carbonaceous material. For example, direct carbonization of nitrile-functionalized thiazolium-based ILs produces carbons that are intrinsically codoped with nitrogen and sulfur heteroatoms.<sup>34</sup> After carbonization at  $1000\text{ }^\circ\text{C}$ , the nitrogen and sulfur contents are as high as 8.75% and 6.98%, respectively. The powder X-ray diffraction (XRD) patterns of the obtained carbons have prominent diffraction lines at  $2\theta$  values between  $24^\circ$  and  $26^\circ$ , representing the typical (002) reflection for graphite-like stacking. Nitrogen and sulfur codoped carbons were also obtained by one-step carbonization of precursor mixtures of common [DCA]-based ILs and an IL containing an isothiocyanate counter-ion ( $[\text{EMIm}][\text{SCN}]$ ).<sup>42</sup> The sulfur content is easily tunable in the range 1.5–3 wt% *via* the initial amount of  $[\text{EMIm}][\text{SCN}]$ . It is worth mentioning that direct carbonization of pure  $[\text{EMIm}][\text{SCN}]$  yields negligible amounts of carbon (5 wt% at  $800\text{ }^\circ\text{C}$  and 0% at  $1000\text{ }^\circ\text{C}$ ).<sup>42</sup> However, this is to be expected, as the thiocyanate trimerizes to thiocyanuric acid, which does not form extended polymer networks, but is sublimated instead.

## 2.2. Conventional ionic liquids

The strategy of direct carbon formation from ILs generally only works for a few, expensive, and, in particular, cyano/nitrile-containing ILs,<sup>24, 25, 31</sup> whereas conventional aprotic ILs without any cross-linkable functional groups under nitrogen and ambient pressure afford no carbon, because of the lack of stable intermediate polymeric structures and the eventual formation of volatile vapors during thermal decomposition of such ILs.<sup>24, 25</sup> Several strategies have been used to deal with this issue. The first approach is to trap conventional ILs in a nanoconfined framework, which is expected to affect pyrolysis and increase aromatization. Similar to the observed abnormal thermal transitions of nanoconfined ILs compared with those of bulk ILs,<sup>44, 45</sup> the confinement of ILs makes the impossible possible, *i.e.*, modifies the carbonization of usually non-carbonizable ILs. For example, introducing the same IL, 1-butyl-3-methylimidazolium bis(trifluoromethylsulfonyl)imide ( $[\text{BMIm}][\text{NTf}_2]$ ), which gives no char residue in the bulk phase into an oxide framework *via* an *in situ* non-hydrolytic sol-gel process affords improved carbonization yields (Figure 5).<sup>43</sup> In addition, by means of the unique solvation environment offered by ILs through coulombic interactions and nanoscopic phase separation, monolithic

silica gels with homogeneously dispersed ILs are liable to produce uniform meso/macropores originating from those of the parent silica-carbon composite, the spaces left by removal of silica, and the interparticle pores between primary carbon particles. The resultant carbon exhibits a surface area of  $469 \text{ m}^2 \text{ g}^{-1}$ .<sup>43</sup> It is believed that aromatization through dehydrogenation reactions is considerably enhanced, and evaporative loss of intermediate species (other than hydrogen gas) is suppressed by the combined effects of nanoconfinement and oxide-catalyzed carbonization. The good energetic interactions between the polar IL precursor and the polar surface of the inorganic template may additionally assist carbonization,<sup>26, 46, 47</sup> as it was reported that commonly non-carbonizable ILs such as [C<sub>8</sub>MIm][Cl], [RMIm][Br], [EMIm][NTf<sub>2</sub>], and [C<sub>4</sub>mpyr][NTf<sub>2</sub>] yielded carbons after carbonization in the presence of inorganic materials such as Fe<sub>3</sub>O<sub>4</sub>, LiFePO<sub>4</sub>, and Li<sub>3</sub>V<sub>2</sub>(PO<sub>4</sub>)<sub>3</sub> nanoparticles, or templates such as monodisperse silica and eutectic salts.<sup>47-53</sup> This confinement-induced carbonization opens the way to carbon synthesis from diverse conventional ILs. The intrinsic nitrogen-containing natures and relatively low carbon yields of such ILs are favorable for the formation of a thin, uniform, conductive, nitrogen-doped carbon layer on the particle surface. In particular, ILs with relatively long carbon chains facilitate adhesion to, and encapsulation of, the inorganic surface, leading to the formation of hollow carbon spheres (HCSs).<sup>47</sup>

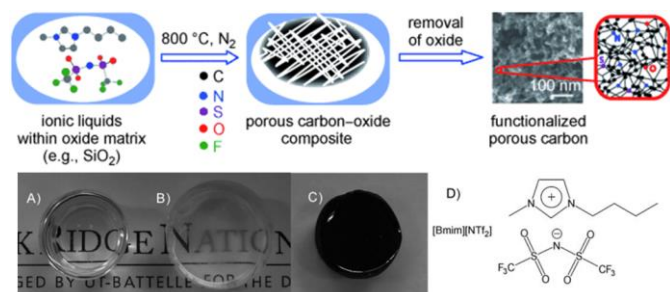


**Figure 5** *In situ* nanoconfinement and carbonization of conventional non-carbonizable ILs. (a, b) Monolithic silica gels before carbonization, (b) after carbonization, and (d) structure of [BMIm][NTf<sub>2</sub>]. [Reprinted with permission from Ref. 43, copyright 2010 Wiley.]

In addition to the nanoconfining method, commonly non-carbonizable ILs can also be transformed into fluorescent carbon dots by fast and simple microwave pyrolysis.<sup>54-56</sup> In this case, the IL acts not only as a carbon source, but also as an excellent medium for absorbing microwaves, because of the high polarizability of the ions in ILs.<sup>57</sup> The obtained carbon dots are small, with a narrow size distribution, *in situ* surface functionalization, and a high quantum yield; they have potential applications such as label-free detection of metal ions.<sup>56</sup>

### 2.3. Poly(ionic liquid)s

Poly-ILs, which are the polymeric form of ILs, and are commonly prepared by polymerization of a monomeric IL using an initiator,<sup>58-61</sup> have also been used as carbon precursors. In spite of the time-consuming polymerization step, poly-ILs show great potential for the preparation of carbon materials. First, unlike the case of IL monomers, for which, because of their fluidic properties, it is difficult to obtain nitrogen-doped carbon materials of designed shapes in the absence of templates,<sup>25, 41</sup> the polymeric nature of poly-ILs enables them to be easily processed. Well-defined morphologies that are inaccessible *via* monomers or small-molecule ILs, such as

fibers and monoliths, can be obtained using poly-ILs.<sup>62, 63</sup> Secondly, polymerization makes it possible to improve the carbon yields from common ILs after appending cross-linking moieties. Thirdly, because of the strong interactions between ILs and organic templates, poly-ILs can homogeneously cover the template surface, by *in situ* polymerization, giving desirable HCSs or carbon-encapsulated structures.<sup>64-68</sup>

**Table 1.** Oven yields of carbons derived from various IL monomers at 1000 °C.

IL	Structure	Yield (%) <sup>a</sup>
IL-0		0 <sup>b</sup>
IL-1		13.0 <sup>c</sup>
IL-2		6.5
IL-3		28.6
IL-4		29.0
IL-5		14.3

<sup>a</sup>Data from ref. 69. <sup>b</sup>Data from ref. 70. <sup>c</sup>Data from ref. 26.

Antonietti and Yuan's group have contributed extensively to the area of poly-IL use as carbon precursors. They first directly carbonized a series of IL monomers containing vinyl or cyano/nitrile groups either in the cation or the anion, and compared their carbon yields.<sup>69</sup> The results, summarized in Table 1, show that in the presence of cross-linking moieties, the IL monomers provide good carbonization yields, which are related to the choice of anion and the alkyl chain on the imidazolium ring. It should be noted that other than the expected cyano/nitrile groups, decorating ILs with vinyl groups can also result in substantial carbon yields and make common ILs containing non-carbonizable anions potential carbon precursors.<sup>67-69</sup> Compared with the popular [EMIm][DCA] (IL-1),<sup>26</sup> IL monomers with an additional vinyl group on the imidazolium ring (IL-3) gave double the carbonization yield (28.6 wt%). Comparisons of IL-2 and IL-3, and IL-2 and IL-4, suggest that the presence of an additional cross-linkable group significantly improves the carbon yield. However, a comparison of IL-4 and IL-5 shows that a longer methylene spacer between the imidazolium core and the cyano group greatly reduces the carbon yield, from 29.0% to 14.3%, probably because of the decrease in the percentage of non-carbonized components. These results show an interesting effect of the precursor structure on the final carbon yield, namely that certain functional groups that undergo cross-linking reactions under pyrolytic conditions significantly improve the carbon yield. Homopolymers were then prepared by conventional free-radical polymerization of IL-2 and IL-3, and successfully carbonized, with carbon yields very close to those of the IL monomers.<sup>69</sup> Thermal polymerization of the IL monomers in the early stages of the reaction may therefore occur

prior to pyrolysis. Although there are great and expected similarities between using IL monomers and polymers as precursors for the pyrolytic formation of carbons, starting from a prepolymerized monomer allows typical polymer operations such as molding, extrusion, coating, or casting with preservation of a given shape to be performed (unlike low-molecular-weight liquids). Such a structured polymer film could then be transferred in a ceramic-like processing step into the final carbon structure.

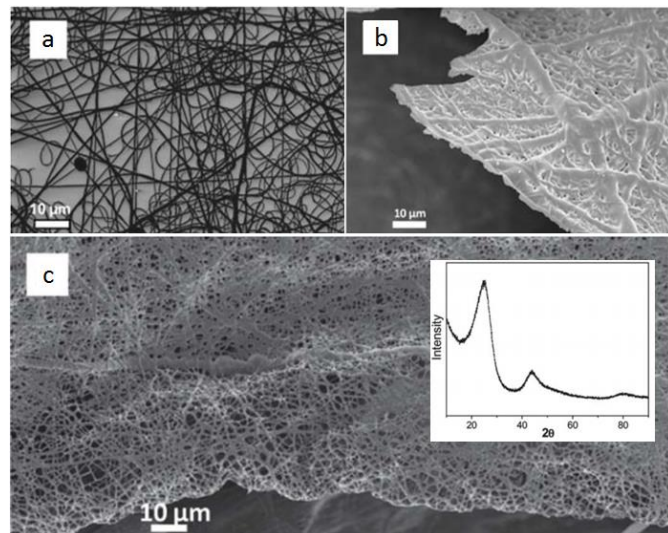


**Figure 6** Scanning electron microscopy (SEM) images of nitrogen-doped (a) carbon fibers and (b) membranes prepared from electrospun PAVIm-DCA fibers, and (c) carbon membranes prepared from electrospun PAVP-DCA fibers. Inset shows the XRD pattern. [Reproduced from Ref. 62.]

Shaped carbon materials can be easily obtained from poly-ILs. Recently, using the well-established electrospinning technique, nitrogen-doped carbon fibers and membranes were obtained from imidazolium- and pyridinium-based poly-ILs as precursors by Yuan *et al.* (Figure 6).<sup>62</sup> However, poly-ILs for electrospinning and carbonization should be carefully designed to solve various problems, in particular, the deformation of polymer chains at elevated temperatures and destruction of the anisotropic shape. The introduction of allyl functions was found to enable poly-IL to cross-link and to maintain their fiber morphology at high temperatures before typical condensation reactions of ILs. In addition, to achieve a high degree of cross-linking, a co-cross-linking agent, *i.e.*, trimethylolpropane tris(3-mercaptopropionate), and a radical initiator, namely 4,4'-azobis(4-cyanovaleric acid), were codissolved with the poly-ILs in an organic solvent. The solution was then subjected to electrospinning followed by carbonization. Figure 6a shows a side view of a monolayer of carbon fibers prepared from an imidazolium-type poly-IL (PAVIm-DCA) on a silicon wafer of diameter 0.2–3 mm. The corresponding carbon membrane, as shown in Figure 6b, displays a homogeneous cross-section membrane structure, of thickness 3–6  $\mu\text{m}$ . In addition, most of the carbon fibers in the membrane maintain the original morphology of the poly-IL fibers. In contrast, the membrane obtained from a pyridinium-type poly-IL (PAVP-DCA) displays structural characteristics different from those of PAVIm-DCA; it is made up of overlapping individual carbon fibers, in a less compact membrane structure, with all the fibers fusing into neighboring ones at the junctions (Figure 6c). The above results demonstrate that the superior processability of poly-ILs and the inherent incorporation of IL moieties in the macromolecular structure can be combined to generate advanced materials with

desired morphologies and complex architectures. In addition, XRD of the membranes indicate that the carbons are graphitic and elemental analysis revealed that PAVIm-DCA and PAVP-DCA carbon fibers doped with 6.33% and 8.0% nitrogen, respectively.

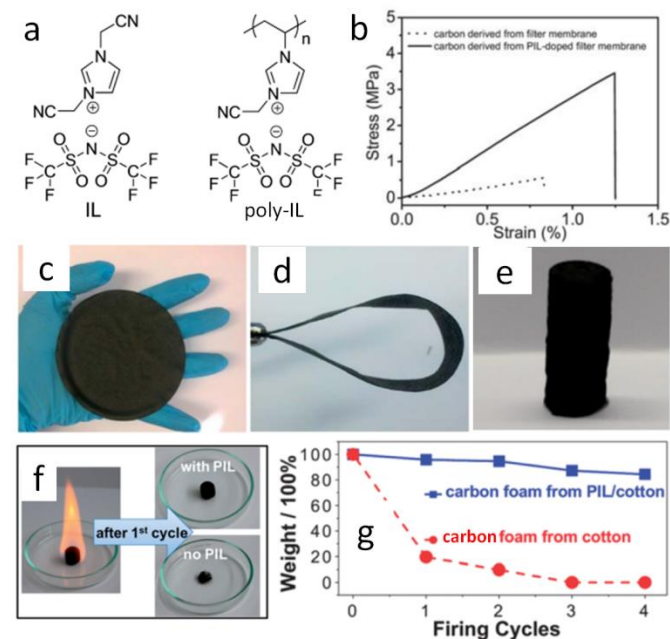


**Figure 7** (a) Chemical structures of IL and poly-IL. (b) Tensile tests of carbon membranes derived from pure cellulose filter membrane (dotted line) and from poly-IL-doped filter membrane (solid line). (c) Carbonaceous membrane paper, (d) bent strip, and (e) monolith derived from poly-IL wetted polysaccharide biomass. (f) Photographs of first firing cycle test of carbon foams. (g) Plot of carbon foam mass vs firing cycle. [Adapted from Ref. 63.]

With the help of low fractions of ILs or poly-ILs, sugar-based molecules and polysaccharide biomass can be turned into functional carbonaceous products at low temperature, *i.e.*, 400  $^{\circ}\text{C}$ , under a nitrogen atmosphere.<sup>63</sup> As shown in Figure 7, flexible, shapable carbonaceous frameworks such as carbonaceous membrane paper, strips, and monoliths were easily obtained by simply coating shaped biotemplates such as cellulose filter membranes, coffee filter paper, or natural cotton with an IL/poly-IL, followed by thermal transformation. These carbonized hybrids exhibit comparably good mechanical properties such as bendability of membranes or shape recovery of foams. Tensile-testing experiments showed that, in contrast to the intact filter membrane, the poly-IL-doped filter membrane gave rise to a carbon membrane with not only a four-fold higher breaking strength, but also a 50% larger rupture strain (Figure 7b). The nitrogen heteroatoms incorporated into the final products from the IL/poly-IL precursors further improve the oxidation stability in fire-retardant tests (Figure 7c and 7d). The “low temperature carbonization/activation” function of ILs/poly-ILs for biomolecules and biomass was further proved by TG analysis of a mixture of IL/ $\beta$ -cyclodextrin ( $\beta$ -CD), which showed a significantly lower onset of mass loss than that of either the IL or  $\beta$ -CD, indicating that a new process resembling chemical activation is involved. Even at a rather low doping ratio (7 wt%), the use of ILs and poly-ILs as activating agents can effectively promote conversion and pore generation in

biomaterials, achieving high surface areas of up to  $720 \text{ m}^2 \text{ g}^{-1}$ . This is attributed to the unique structures of ILs and poly-ILs; both contain a bulky anion,  $[\text{NTf}_2]$ , and one or two cyanomethyl groups attached directly to the imidazolium cation (Figure 7a). Such a chemical combination is known to readily form porous carbons on pyrolysis, without any external template or activating agent.<sup>25, 39</sup> Carbon monoliths can also be prepared by one-pot solvothermal copolymerization of IL monomers with divinylbenzene and subsequent carbonization in a  $\text{CO}_2$  atmosphere.<sup>65</sup>

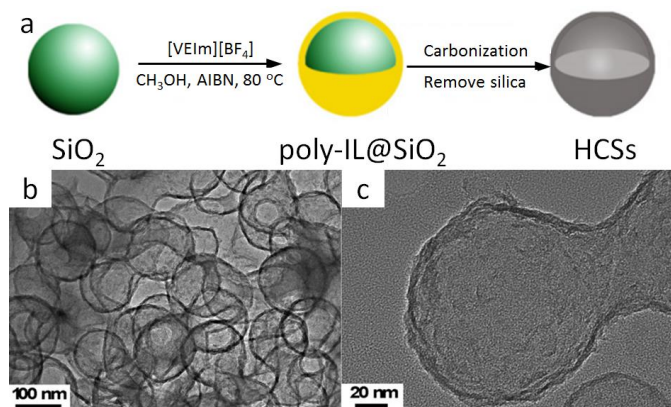


**Figure 8** (a) Preparation of HCSs and (b, c) TEM images of HCSs. [Reprinted with permission from Ref. 67, copyright 2011 Elsevier.]

The known favorable interactions between the strongly polar IL monomers and polar inorganic silica templates undoubtedly facilitate the synthesis of high-surface-area, nitrogen-doped carbons with various morphologies.<sup>46</sup> HCSs can be easily fabricated using poly-ILs as carbon precursors and monodisperse silica particles as templates.<sup>67, 71</sup> The overall procedure for HCS preparation is presented in Figure 8a. First, the IL monomer (1-vinyl-3-ethylimidazolium tetrafluoroborate,  $[\text{VEIm}][\text{BF}_4]$ ) was coated on the surfaces of monodisperse silica particles, accompanied by *in situ* polymerization. The obtained core/shell composite spheres with a uniform poly-IL layer were then carbonized, with subsequent template removal, generating carbon spheres with hollow structures. Transmission electron microscopy (TEM) images (Figure 8b and 8c) show that the HCSs are made up of hollow spheres with shells of thickness 7 nm, and hollow cores of size 105 nm, consistent with the diameter of the silica template. Following a very similar strategy, but replacing the monomer IL by one containing both cyano and vinyl groups, Yuan *et al.* successfully prepared porous nitrogen-doped HCSs with tailored particle sizes, nitrogen contents, and wall thicknesses, which are partially graphitized and exhibit hierarchical pore structures and size-dependent surface areas of up to  $570 \text{ m}^2 \text{ g}^{-1}$ .<sup>64</sup> The strategy for synthesizing nitrogen-doped carbon layers by *in situ* polymerization of monomer ILs can be expanded to other nanosubstrates such as carbon nanotubes (CNTs).<sup>68</sup> Instead of *in situ* polymerization, the as-synthesized poly-ILs are directly deposited on a template such as colloidal silica using layer-by-layer assembly.<sup>66</sup> Subsequent carbonization and template removal produce carbon capsules containing ca. 7 wt% nitrogen, with a surface area of  $423 \text{ m}^2 \text{ g}^{-1}$ .

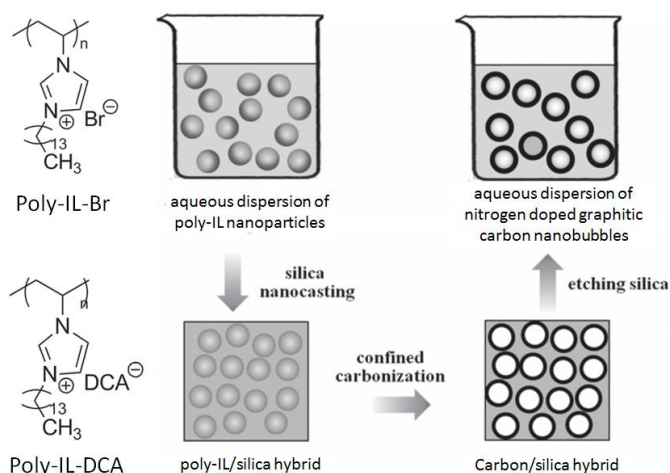


**Figure 9** Chemical structures of poly-IL nanoparticles and synthetic route to nitrogen-doped carbon nanobubbles by confined carbonization of poly-IL nanoparticles in a silica matrix. [Reprinted with permission from Ref. 72, copyright 2013 Wiley.]

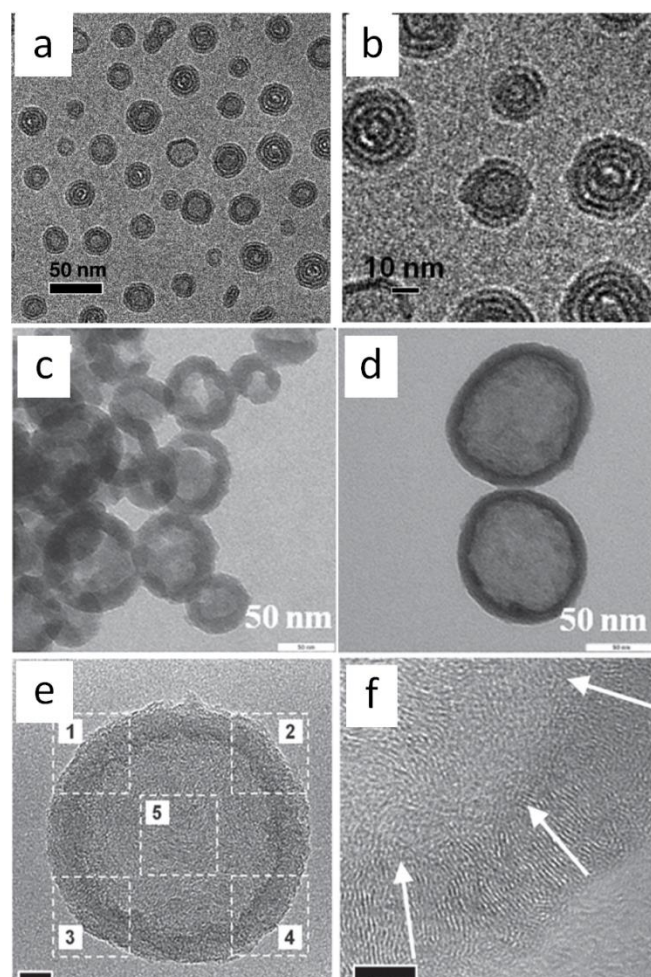


**Figure 10** (a, b) Cryo-TEM images of poly-IL-Br nanoparticles in aqueous solution. [Reprinted with permission from Ref. 73, copyright 2011 American Chemical Society.] (c, d) TEM images of nitrogen-doped carbon nanobubbles prepared from poly-IL-Br and poly-IL-DCA, respectively. (e) TEM image of a single nitrogen-doped carbon nanobubble. (f) HRTEM image of a single nitrogen-doped carbon nanobubble.

part 4 in Figure 10e. The white arrows indicate the planar direction of the stacked graphenes. [Reprinted with permission from Ref. 72, copyright 2013 Wiley.]

In addition, in an inverse strategy to encapsulating a silica template by poly-ILs to obtain a nitrogen-doped carbon layer, carbon nanobubbles with controlled dimensions, variable nitrogen doping, superior aqueous dispersibility, high conductivity, and a distinctive atomic graphitic order were obtained using poly-IL nanoparticles with a triple role, namely sacrificial template, carbon precursor, and nitrogen source, with silica as a solidifying agent.<sup>72</sup> The structures of the poly-ILs and the overall synthetic routes are shown in Figure 9. Spherical poly-IL nanoparticles in aqueous solution were obtained *via* simultaneous polymerization/self-assembly of IL monomers with long alkyl chains.<sup>73, 74</sup> It was assumed that the as-formed poly-IL nanoparticles were probably assembled in organized mesophases consisted of separate nanodomains of charged IL moieties and long hydrophobic alkyl chains. As seen in Figure 10a and 10b, the poly-IL-Br nanoparticles have a number of spontaneously formed bilayers as well as a central “void”, the size of which is independent of the bilayer number.<sup>58</sup> Silica nanocasting was performed by dropwise addition of a liquid silica precursor such as tetraethyl orthosilicate, followed by hydrolysis and condensation. The poly-IL/silica composite was then subjected to carbonization and template removal, yielding porous HCSs (Figure 10c and 10d). It should be noted that nanoconfinement of the poly-IL in the solidified silica reservoir greatly enhanced the carbonization yields, which were similar to that reported by Dai *et al.*<sup>43</sup> For example, a carbon yield of up to 30% was achieved for poly-IL-DCA nanoparticles, which is more than twice that for non-confined carbonization of poly-IL-DCA (13%). Based on the anion type in the poly-IL nanoparticles ([Br] or [DCA]), and the type of liquid silica precursor, the nitrogen content and the size of the nanobubble are tunable over a wide range. Highly graphitic three-dimensional nanostructures with special local organization were observed in the resultant carbons. As seen in Figure 10e and 10f, high-resolution (HR) TEM images of the carbon derived from poly-IL-DCA showed a layer-like pattern stemming from stacking of slightly distorted graphene layers. Independent of the specific position, these graphene layers are essentially oriented perpendicularly to the nanosphere surface, *i.e.*, all the layers point to the nanosphere center. Although each layer appears parallel to its neighbor, the graphene sheet shifts its orientation slightly *via* step defects, so a short distance of several nanometers produces a detectable tilt. Along the nanosphere circumference, the graphene director basically rotates through 360°.

In addition, poly-ILs were shown to improve the hydrothermal carbonization of ordinary sugars in terms of the structures, properties, and functions of the carbon products, which are porous, nitrogen-containing, and composed of primary spherical nanoparticles. In particular, compared with the carbon products derived from pure sugars or with IL additives with very low surface areas (<10 m<sup>2</sup> g<sup>-1</sup>), the use of poly-IL additives, at weight fractions of 0.55–13.3%, significantly increased the surface areas to 161 m<sup>2</sup> g<sup>-1</sup> for hydrothermal carbonization materials and 572 m<sup>2</sup> g<sup>-1</sup> for post-carbonization materials. The poly-ILs are therefore believed to act not only as nitrogen sources, but also as stabilizers and pore-generating agents.<sup>75</sup>

#### 2.4. Deep-eutectic solvents

DESs are mixtures for which the freezing point is lower than that of either of its individual components; they can be generally obtained by complexation of quaternary ammonium salts with hydrogen-bond donors such as acids, amines, and alcohols,<sup>76, 77</sup> or even obtained by direct combination of amides and inorganic salts.<sup>78</sup> DESs have recently been described as a new class of ILs, because they share many characteristics with conventional ILs, but their low cost makes them particularly desirable for use in the large-scale synthesis of new functional materials.<sup>77, 79-81</sup>

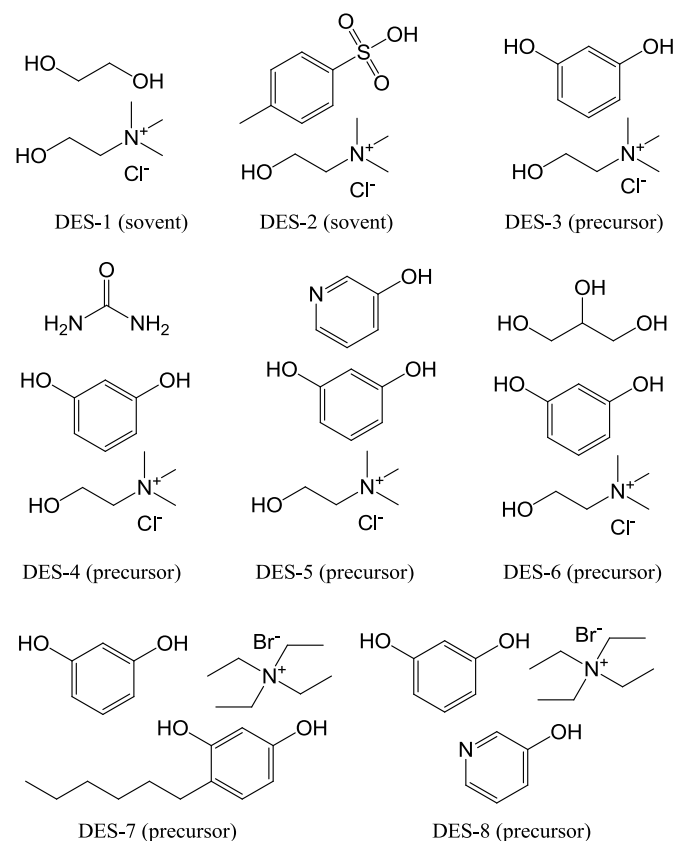


**Figure 11.** Structures of DESs used for synthesis of carbon materials. Description in parentheses indicates the corresponding role during polycondensation and carbonization.

Monte *et al.* performed pioneering work in the field of synthesis of carbon materials from DESs.<sup>82-90</sup> In 2010, they explored the suitability of DESs based on a mixture of ethylene glycol and choline chloride (molar ratio 2:1, DES-1, Figure 11) to achieve the polycondensation of resorcinol with formaldehyde.<sup>82</sup> However, the DES investigated in this work, because of its thermal instability, was demonstrated to be not a real carbon precursor, but a simple solvent and a catalyst that can promote the polycondensation of resorcinol–formaldehyde. A DES based on *p*-toluenesulfonic acid and choline chloride (DES-2, Figure 11) was also prepared and used as a solvent, acidic catalyst, and structure-directing agent to assist the condensation of furfuryl alcohol, with subsequent carbonization. This DES is also an excellent solvent for homogeneously dispersing CNTs, finally resulting in hierarchical porous composites with a homogeneous distribution of CNTs throughout the entire monolithic structure.<sup>89</sup> Following on from this work, Monte *et al.* further synthesized a new type of DES by replacing the previous

hydrogen-bond acceptors (ethylene glycol and *p*-toluenesulfonic acid) with resorcinol, a regular carbonaceous precursor for formation of resorcinol–formaldehyde resins by polycondensation (DES-3 to DES-8, Figure 11). For example, resorcinol-based DESs with or without urea (DES-3 and DES-4) were directly used to prepare hierarchical porous carbon monoliths *via* formaldehyde polycondensation and subsequent carbonization.<sup>83</sup> The DESs played multiple roles in the synthetic process, *i.e.*, a liquid medium ensuring reagent homogenization, a carbonaceous precursor *via* formaldehyde polycondensation and subsequent carbonization, and a structure-directing agent *via* choline chloride segregation in a spinodal-like decomposition process, which is responsible for achievement of the hierarchical structure. One attractive feature is that self-contained resorcinol in the DESs requires no other phenolic additives for polycondensation and carbonization. The resorcinol becomes the material itself, with high carbon conversion, and the choline chloride can be recovered and reused in subsequent reactions, making DES-assisted syntheses very efficient in terms of reagent economy. Carbon conversion of resorcinol-based DESs was as high as 80%. Moreover, carbon monoliths with high surface areas, up to 612 m<sup>2</sup> g<sup>-1</sup>, bimodal pores (micropores and mesopores), and narrow mesopore diameter distributions were obtained. The urea composition in the DESs can further expand the mesopore size to 23 nm. Since the urea component in DES-4 is released during carbonization, Monte *et al.* synthesized new DESs containing 3-hydroxypyridine as the nitrogen source in the carbon (DES-5, Figure 11).<sup>86</sup> Carbon monoliths with high nitrogen contents, high surface areas, and high carbon conversions (above 70%) were obtained *via* a formaldehyde polycondensation and carbonization process similar to that used with previous DESs. Scanning electron microscopy (SEM) images showed that the resulting carbon morphology consisted of a bicontinuous porous network built of highly cross-linked clusters that aggregated and assembled into a stiff, interconnected structure (Figure 12). Furthermore, on addition of phosphoric acid as a catalyst during polycondensation of DES-6, phosphate-functionalized carbon monoliths were obtained after carbonization of the unwashed phenolic resin, which had a phosphorous content of about 8 wt%, determined using energy-dispersive X-ray spectroscopy (EDX), and a micropore surface area of about 600 m<sup>2</sup> g<sup>-1</sup>, calculated using a *t*-plot, making it highly suitable for electrodes in supercapacitors.<sup>84</sup>

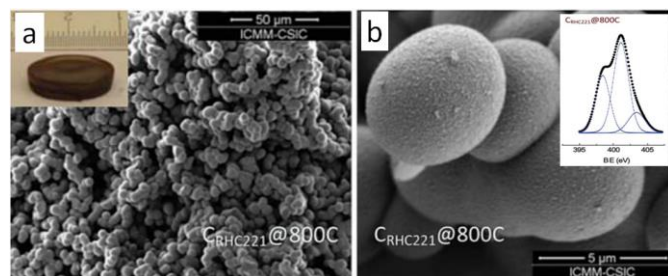


**Figure 12.** SEM micrographs of nitrogen-doped hierarchical carbon obtained from DES-5. Insets show photograph of the carbon monolith and high-resolution N1s X-ray photoelectron spectra (XPS), respectively. [Adapted from Ref. 86.]

Using long-alkyl-chain 4-hexylresorcinol and tetraethylammonium bromide as the co-hydrogen donor and hydrogen acceptor, respectively, the as-formed DES-7 (Figure

11) was capable of providing microporous carbon monoliths. Notably, all the resultant carbons showed particularly narrow microporosities, with an average micropore diameter of ca. 0.6 nm. This narrow microporosity gave rise to negligible N<sub>2</sub> uptake and a low surface area (<7 m<sup>2</sup> g<sup>-1</sup>), but they did exhibit high adsorption of CO<sub>2</sub> (2.2 mmol g<sup>-1</sup> at 25 °C). The selective adsorption of CO<sub>2</sub> was ascribed to the molecular sieve character of these carbons, so gases with small kinetic diameters (*e.g.*, 0.33 nm for CO<sub>2</sub>) are preferentially adsorbed over those with large ones (*e.g.*, 0.36 nm for N<sub>2</sub> or 0.38 nm for CH<sub>4</sub>).<sup>85</sup> Hierarchical porous nitrogen-doped carbons were obtained from DES-8, composed of resorcinol, 3-hydroxypyridine, and tetraethylammonium bromide, in which 3-hydroxypyridine acted as the nitrogen source in the resulting carbons, and tetraethylammonium bromide determined the formation of a molecular sieve structure.<sup>87</sup> Varying the carbonization temperature and molar ratio between each component can tailor the hierarchical-type porous structure to give macro- and micropores, and to control the nitrogen content up to 8.7 wt%. Finally, a high and selective CO<sub>2</sub> adsorption capacity over N<sub>2</sub> (2.7 mmol g<sup>-1</sup> at 25 °C) was achieved.

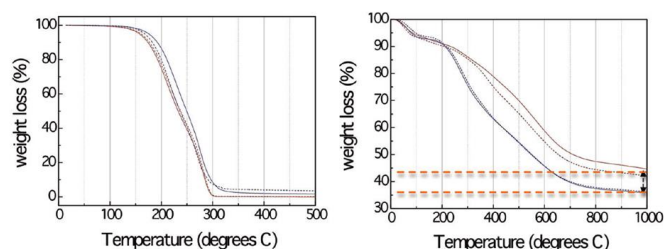


**Figure 13** TG profiles of (left) DESs and (right) corresponding resorcinol–formaldehyde gels derived from DES-3 and DES-4. [Reprinted with permission from Ref. 83, copyright 2010 American Chemical Society.]

Although DESs show great potential as carbon precursors, such as low cost, and ease of production of bulk monolithic carbons with hierarchical porous and interconnected hierarchical structures, the direct carbonization of DESs without polycondensation resulted in no carbon residues. TG analysis (Figure 13) confirmed that compared with the formed resorcinol–formaldehyde gels, even the DESs containing an aromatic component (resorcinol) are nearly completely decomposed below 300 °C.<sup>83</sup> A possible reason is the relatively weak hydrogen-bond strength between the hydrogen donors (amines and alcohols) and acceptors (halogen anions), which makes DESs thermally unstable prior to preliminary polymerization and carbonization at high temperature. The unavoidable use of toxic formaldehyde for polycondensations with very long reaction times (usually 1 week) in the synthesis of porous carbon using the soft template method involving formaldehyde and phenol, resorcinol, or phloroglucinol<sup>18</sup> undoubtedly may hinder its widespread application.

## 2.5. Protic ionic liquids and salts

As mentioned above, although cyano/nitrile-containing ILs show great potential for carbon materials, very few cyano/nitrile-containing aprotic ILs yield carbons.<sup>24, 25</sup> Moreover, the multistep and time-consuming synthesis,

rigorous purification, metal impurities (*e.g.*, Li, Na, or Ag, possibly from metathesis), and high cost complicate their manufacture and inevitably hinder large-scale production.

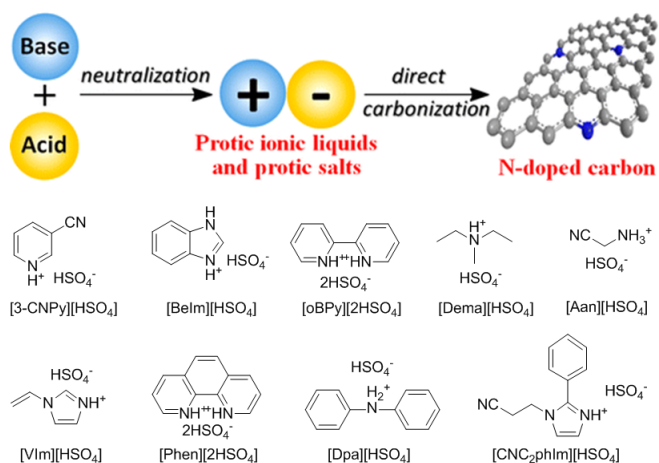


**Figure 14** Schematic representation of synthesis of carbon materials by direct carbonization of PILs/PSs and Structures of the typical PILs/PSs. [Reprinted with permission from Ref. 91, copyright 2014 American Chemical Society.]

Based on the previous finding that 1,8-diazabicyclo[5.4.0]undec-7-ene-based PILs can bear relatively high-temperature treatment (500 °C), with residual yields of up to 25%,<sup>92</sup> Watanabe *et al.* recently found that nitrogen-containing PILs and PSs have great potential as single, low-cost, and versatile precursors for the facile one-step synthesis of carbon materials, without any complicated synthesis, catalyst, prepolymerization or other complex techniques.<sup>91, 93</sup> Unlike the specific aprotic ILs limited to those with cyano/nitrile moieties, PILs/PSs that tolerate harsh carbonization conditions can be easily prepared and are cheap. As shown in Figure 14, the whole process is simple and rapid, involving only two steps, *i.e.*, neutralization and carbonization. Instead of the expected complete weight loss of the parent bases below 400 °C, the carbon yields from the PILs/PSs depended strongly on the base structures. The unique compositions of all the PILs/PSs discussed here enable *in situ* fabrication of intrinsic nitrogen-doped carbons, with nitrogen contents varying significantly, depending on the precursors. In particular, the carbon derived from [3-CNPy][HSO<sub>4</sub>] has a very high nitrogen content of 11.1 wt% after carbonization at 1000 °C. Considering that [3-CNPy][HSO<sub>4</sub>] has a N/C molar ratio of 0.33, only half that of [EMIm][DCA] (0.63),<sup>26</sup> the high nitrogen content observed in the resulting carbon is surprising, and indicates that at least 30% of the nitrogen atoms originally present in the [3-CNPy][HSO<sub>4</sub>] precursor were finally incorporated within the carbon architecture.

Most of the highly nitrogen-doped carbons, *i.e.*, [3-CNPy][HSO<sub>4</sub>]-, [Phen][2HSO<sub>4</sub>]-, and [CNC<sub>2</sub>phIm][HSO<sub>4</sub>]-based carbons, despite their very high nitrogen contents, are more graphitic than carbons with lower N contents, shown by the more positive shift of the diffraction position, higher intensity, and narrower line width of the (002) peak (Figure 15a). In particular, the [CNC<sub>2</sub>phIm][HSO<sub>4</sub>]-derived carbon shows a high-intensity (002) diffraction peak centered at 26.2°. The calculated interlayer distance ( $d_{002}$ ) of 0.339 nm is comparable to that of graphite (0.335 nm).<sup>94</sup> HRTEM showed local organization of graphitic carbons, in which bent graphite-

like sheets are uniformly present throughout the entire carbon structure. Interestingly, the graphene layers in the [CNC<sub>2</sub>phIm][HSO<sub>4</sub>]-based carbon are mostly arranged in one direction, because of its high degree of graphitization, whereas in the case of [3-CNPy][HSO<sub>4</sub>], the graphene layers are much more randomly oriented (arrows in Figure 15c and 15d). In contrast, the [oBPy][2HSO<sub>4</sub>]-based carbon, with a high nitrogen content, is more amorphous, as revealed by the weak, broad (002) signal. The differences were checked using XPS. The results showed that the carbons from [3-CNPy][HSO<sub>4</sub>], [CNC<sub>2</sub>phIm][HSO<sub>4</sub>], and [Phen][2HSO<sub>4</sub>] have high percentages of pyridinic nitrogen but low percentages of quaternary nitrogen. The former is known to be planar, whereas the latter has an out-of-plane bonding configuration.<sup>95</sup> The above three carbons with high percentages of pyridinic nitrogen, with planar structures, therefore have short interlayer distances and are more graphitic.

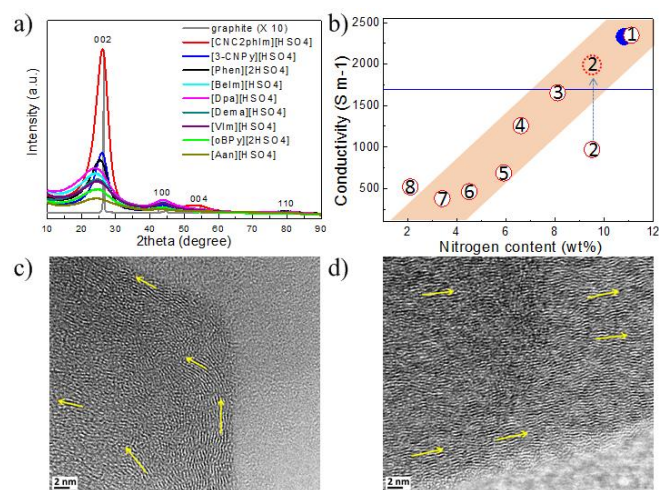


**Figure 15** (a) XRD patterns and (b) relative conductivities of carbons derived from PILs/PSs. 1: [3-CNPy][HSO<sub>4</sub>], 2: [oBPy][2HSO<sub>4</sub>], 3: [CNC<sub>2</sub>phIm][HSO<sub>4</sub>], 4: [Phen][2HSO<sub>4</sub>], 5: [Belm][HSO<sub>4</sub>], 6: [Dpa][HSO<sub>4</sub>], 7: [VIm][HSO<sub>4</sub>], and 8: [Dema][HSO<sub>4</sub>]. Red dashed circle indicates estimated conductivity of carbon 2 from general relationship between nitrogen content and conductivity. [EMIm][DCA]-based carbon and graphite are shown by blue solid circle and line, respectively. HRTEM images of carbons derived from (e) [3-CNPy][HSO<sub>4</sub>] and (f) [CNC<sub>2</sub>phIm][HSO<sub>4</sub>]. [Reprinted with permission from Ref. 93, copyright 2014 American Chemical Society.]

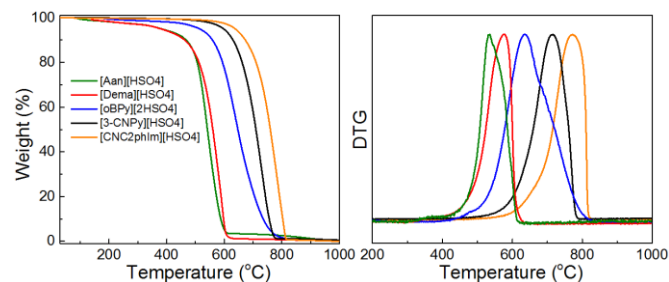


**Figure 16** TG curves of PIL/PS-derived carbon materials in air (heating rate: 10 °C min<sup>-1</sup>). Decomposition temperature was determined from differential TG peak. [Reprinted with permission from Ref. 91, copyright 2014 American Chemical Society.]

Interestingly, a nearly linear relationship between the nitrogen contents and electrical conductivities of the PIL/PS-based carbons was observed. As shown in Figure 15b, the conductivity is roughly proportional to the nitrogen content (orange region in Fig. 2d), because of the doping effect of electron-rich nitrogen, which induces a donor state above the Fermi energy level and increases its electron density.<sup>30, 96, 97</sup> For [3-CNPy][H<sub>2</sub>SO<sub>4</sub>]-based carbon, which has the highest nitrogen content and relatively high degree of graphitization, the conductivity is even higher than that of graphite, showing similar results to those for [EMIm][DCA]-based carbon.<sup>26</sup> In contrast, [oBPy][2H<sub>2</sub>SO<sub>4</sub>]-based carbon, despite its high nitrogen content (9.5 wt%), exhibits much lower conductivity than expected (Figure 15b). The graphitic structures and nitrogen contents of PIL/PS-derived carbons can both affect the thermal stability against oxidation, although the observed trend in the thermal stabilities of PIL/PS-derived carbons is slightly different from that of the conductivities. In the case of the thermal stabilities, graphitization of the carbon material significantly improves its thermal stability in air. As seen in Figure 16, the [CNC<sub>2</sub>phIm][H<sub>2</sub>SO<sub>4</sub>]-based carbon, which has the highest degree of graphitization and a relatively high nitrogen content (8.1 wt%), has a much higher decomposition temperature (ca. 773 °C) than the others. The effect of graphitization is further shown by the lower decomposition temperature (635 °C) for [oBPy][H<sub>2</sub>SO<sub>4</sub>]-based carbon, although its nitrogen content (9.5 wt%) is higher than that of [CNC<sub>2</sub>phIm][H<sub>2</sub>SO<sub>4</sub>]-based carbon. [Dema][H<sub>2</sub>SO<sub>4</sub>]- and [Aan][H<sub>2</sub>SO<sub>4</sub>]-based carbons, which both have low nitrogen contents (2.1 and 2.7 nitrogen wt%) and graphitization, showed lower-temperature weight-loss profiles, at 577 and 534 °C, as expected.<sup>91</sup>

In addition, depending on the precursor structure, the obtained carbon materials vary from non-porous to microporous. Some of them exhibit high surface areas of up to 1380 m<sup>2</sup> g<sup>-1</sup>. Highly porous carbon can only be obtained *via* nanocasting or activation, therefore this facile one-step method is of great significance. The carbonization mechanism was investigated using [CNC<sub>2</sub>phIm][H<sub>2</sub>SO<sub>4</sub>] as a typical precursor containing various distinct but common moieties present in most PILs/PSs. It was found that during carbonization, the thermally unstable moieties such as alkyl chains, cyano functional groups, anions, and heterocyclic imidazolium rings decomposed at low temperature, and the fragments formed *in situ* then underwent a number of transformations such as cross-linking polymerization and recombination, partially condensed and/or fused with the thermally stable domains to form nitrogen-containing polycyclic aromatic compounds, and were finally transformed into nitrogen-doped carbon. Notably, the high proton-transfer energy between the protic acid and base, which is much higher than those of DESs, is essential to improve the thermal stabilities of the PILs/PSs and ensure high carbon yields under harsh carbonization conditions.<sup>92</sup>

This PIL/PS-based strategy was used to synthesize and directly carbonize a series of PILs/PSs with various nitrogen-containing bases and acids.<sup>91</sup> The nitrogen-containing bases investigated were aliphatic amines, aromatic amines, and heterocycles, with or without unsaturated C=C bonds or cyano groups, and the acids were common inorganic and organic acids. Because of the wide availability of the PIL/PS precursors and their diverse structures, the general correlations between the carbonaceous precursors and resultant carbon materials, in terms of carbon yield, graphitic structure, nitrogen content, and

porosity, have been investigated in detail; the results are summarized below.

- High carbon yields** can be obtained from PILs/PSs with high proton-transfer energies, which prevent the reverse reaction to form neutral acids and bases. In addition, thermally stable domains such as fused aromatic moieties, benzene groups, or unsaturated bonds help to improve carbon yields.
- Carbons with high nitrogen contents** can be obtained from PIL/PS precursors with relatively high C/N ratios (usually C/N is 3–5), but not from those with extremely high nitrogen contents (*e.g.*, C/N < 1). The incorporation of structural nitrogen such as pyridine, imidazole, CN, and thermally stable C=N moieties may additionally increase the number of the expected functional nitrogen species, but aliphatic amines containing unstable C–N bonds do not contribute significantly to the nitrogen content.
- Carbons with high surface areas** can be obtained from PIL/PS precursors containing unstable moieties such as aliphatic chains or heterocyclic rings; most of the nitrogen-containing bases and anions are sacrificed as porogens or templates to generate large amounts of pores.
- Carbons with high degrees of graphitization** can be obtained from PIL/PS precursors simultaneously containing a heterocycle, a CN group, and an aromatic structure; at least a heterocycle and CN group is required. However, establishing a firm correlation between the chemical structures of PILs/PSs and the carbon characteristics remains a challenge for the future.

These conclusions show that these low-cost and versatile precursors pave the way for the design and synthesis of task-specific carbon materials through rational design and selection of bases, acids, and functional groups. In fact, most of the above points hold true for aprotic ILs and neutral precursors.

### 3. Ionic liquids as surface-coating agents, dopants, and media for carbon materials

#### 3.1. Ionic liquids as surface-coating agents

The promising liquid features of IL precursors coupled with the high nitrogen contents and graphitic structures of the resultant carbons make [DCA]-based ILs ideal precursors. However, the relatively low carbon yield (<13% at 1000 °C) and high cost strongly hinder large-scale production. In particular, compared with carbon materials derived from conventional precursors, those formed from ILs are expensive. The carbon yield can be improved using the aforementioned nanoconfinement method. Regarding the high cost, an alternative method is to decorate the surfaces of bulk materials with a thin layer of IL-derived nitrogen-doped carbons; this reduces the absolute amount of IL required, but maintains the attractive features of IL-derived carbons, such as high conductivities and nitrogen contents.

Hu *et al.* recently used ILs as precursors for the formation of carbon coatings on Li<sub>4</sub>Ti<sub>5</sub>O<sub>12</sub> electrodes for LIBs.<sup>53, 98</sup> The composite material was obtained by simply mixing [EMIm][DCA] with pristine Li<sub>4</sub>Ti<sub>5</sub>O<sub>12</sub>, accompanied by carbonization. The HRTEM image in Figure 17a shows that a very thin uniform amorphous layer is formed on the surface of the anode material. The EDX mapping images (Figure 17b) show that the distribution of carbon and nitrogen elements is consistent with that of Ti, indicating a uniform nitrogen-doped

carbon coating on/in the particles. The resultant composite  $\text{Li}_4\text{Ti}_5\text{O}_{12}$  electrode coated with a thin, conductive, nitrogen-doped carbon layer has a superior rate capability and cycling performance versus Li compared with the pristine sample.<sup>95</sup> [EMIm][DCA] was also used to coat a Pt/XC-72 catalyst with a nitrogen-doped carbon layer; the coating structure not only improved the charge-transfer rate at the metal-support interface, but also promoted dispersion and reduced agglomeration of Pt nanoparticles. The resultant catalysts exhibited considerable electrochemical surface areas and significant electrocatalytic activity in methanol oxidation compared with the uncoated catalysts.<sup>99</sup> In addition, nitrogen-doped-carbon-coated CNTs were obtained through pyrolyzing IL precursors on the surfaces of commercial CNTs, using either a typical carbonizable IL ([EMIm][DCA])<sup>100</sup> or *in situ* polymerization of IL monomers.<sup>68</sup> In the latter case, the TEM image revealed that after polymerization and carbonization, a thin amorphous carbon layer ( $\text{CN}_x$ ) of thickness ca. 1.5 nm covered the CNT side walls (Figure 18). The resultant surface-nitrogen-enriched CNTs (SNE-CNTs) were demonstrated to be potential supports for noble-metal nanoparticles for electrocatalysis. This strategy for obtaining SNE-CNTs introduces a high content and uniform distribution of nitrogen atoms in the shell, enabling the CNT surface to anchor and grow noble-metal nanoparticles, while maintaining the electronic conductivity and structure of the core CNT.

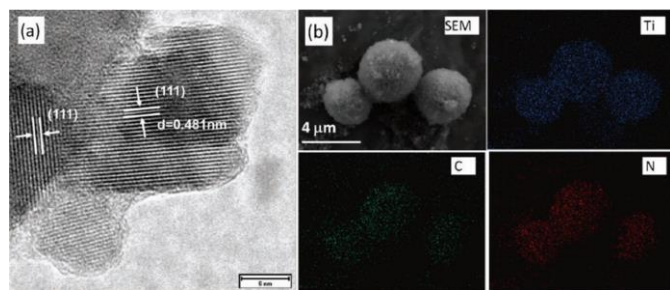


**Figure 17** (a) HRTEM and (b) SEM and EDX mapping images of Ti, carbon, and nitrogen elements in coated  $\text{Li}_4\text{Ti}_5\text{O}_{12}$ . [Reprinted with permission from Ref. 98, copyright 2011 Wiley.]

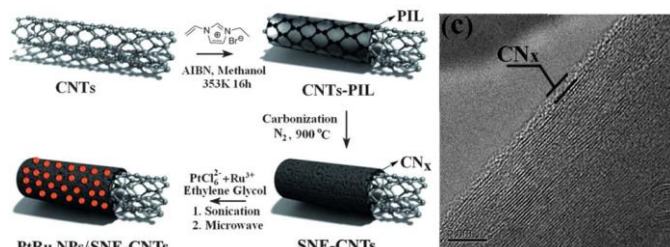


**Figure 18** Schematic diagram of preparation of SNE-CNTs and PtRu nanoparticle/SNE-CNT nanohybrids, and TEM images of CNT-PIL (a) and SNE-CNT (b, c) nanocomposites. [Adapted from Ref. 68.]

### 3.2. Ionic liquids as heteroatom dopants

Another method for reducing the IL amount but retaining the performance of nitrogen-doped carbon is to use ILs as heteroatom dopants in the synthesis of carbon materials from other inorganic [e.g., graphene or graphene oxide (GO)] or organic carbonaceous precursors (e.g., a polymer).<sup>101-105</sup> For example, ILs can function as both nitrogen dopants and shape-

directing agents for the synthesis of microporous carbon nanosheets from GO and resorcinol-formaldehyde polymers.<sup>101</sup> As shown in Figure 19a, the carbon sheets obtained in the presence of IL consist of two parts, with the inner graphene layer coated with carbon on both sides. No free carbon particles or naked graphene sheets are observed in SEM images, suggesting perfect assembly of resorcinol, formaldehyde, and the ILs on the surfaces of the GO sheets; this was confirmed by the uniform distribution of nitrogen on the carbon surface indicated by EDX mapping images. In contrast, in the absence of an IL, the carbon sheets stack on top of each other, resulting in serious aggregation (Figure 19b).<sup>101</sup> Nitrogen-doped graphene with a N/C molar ratio and electrical conductivity of 22.1% and  $7.15 \times 10^4 \text{ S m}^{-1}$ , respectively, can be synthesized by IL-assisted electrolysis with subsequent thermal annealing of the IL-functionalized graphene sheets. The surface properties such as the nitrogen configuration can be controlled by changing the anion ([Br], [AC], and [PF<sub>6</sub>]).<sup>104</sup> In addition, nitrogen and boron codoped porous carbons with fully connected three-dimensional hierarchical porosities and local graphitic textures were derived from poly(benzoxazine-co-resol) polymers, using the IL [C<sub>16</sub>MIm][BF<sub>4</sub>] as an additive. Use of the IL not only leads to heteroatom incorporation into the framework, but also modulates the carbon microstructure.<sup>105</sup>

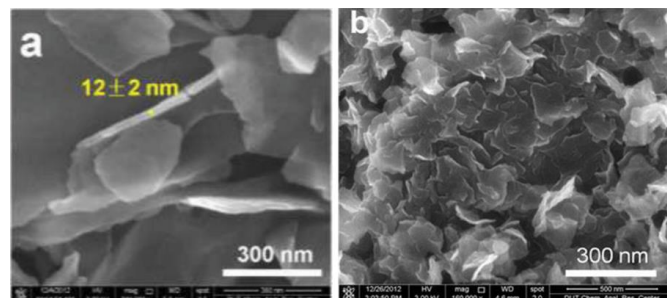


**Figure 19** Field-emission SEM images of NMCS samples synthesized in (a) presence and (b) absence of 1-butyl-3-methylimidazolium imidazolide ([BMIm][Im]). [Reprinted with permission from Ref. 101, copyright 2014 Wiley.]

### 3.3. Ionic liquids as media, solvents, and soft templates

As well as acting as dopants, ILs can also be used as media, solvents, or even soft templates in the formation of carbon materials.<sup>106-112</sup> The ILs may be partially incorporated into the final carbon materials during carbonization. For example, cothermal condensation of [BMIm][BF<sub>4</sub>] and dicyandiamide was used to synthesize a new type of boron- and fluorine-enriched polymeric carbon nitride. Notably, the resulting materials have the technically advantageous “morel-like” mesoporous structure, with a narrow pore size distribution (Figure 20); this originates from the IL as a soft template. These materials exhibit good photoactivities under visible-light illumination and good catalytic performances in the selective oxidation of cycloalkanes.<sup>106</sup>

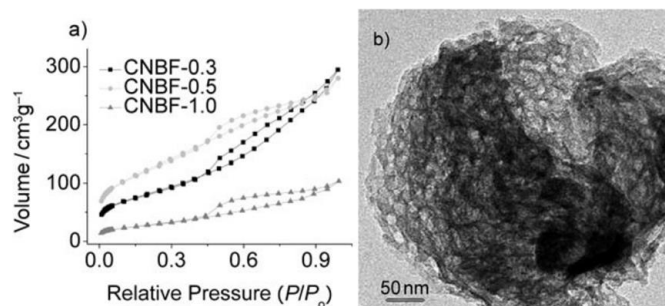


**Figure 20** Nitrogen adsorption–desorption isotherms and TEM image of boron- and fluorine-enriched polymeric carbon nitride. [Reprinted with permission from Ref. 106, copyright 2010 Wiley.]

ILs can be used as alternatives to traditional reaction media (e.g., H<sub>2</sub>O) in the ionothermal synthesis of carbon materials from biomass at ambient pressure.<sup>110, 113</sup> For example, mesoporous carbons have been synthesized by ionothermal carbonization of glucose or fructose in PILs at low temperatures under ambient pressure.<sup>110</sup> Three factors are considered to be key to the success of the ionothermal approach. First, the low vapor pressure of the PIL maintains a stable reaction environment, without solvent vaporization, and avoids the use of autogenic reaction systems. Secondly, the latent acidity of the PIL catalyzes the dehydration of fructose and glucose. Finally, the PIL significantly enhances the solubility of sugars with abundant hydroxyl groups *via* enhanced hydrogen-bonding interactions.<sup>110</sup> Lewis acidic metal-containing ILs such as [BMIm][FeCl<sub>4</sub>] can also play a “three-in-one” role (soft template, solvent, and catalyst) in the synthesis of hierarchical porous carbonaceous materials.<sup>113</sup> Porous carbon aerogels were obtained from resorcinol–formaldehyde resin without a supercritical drying process, using ILs as soft templates.<sup>108</sup> Both the structure (different side chains or anions) and amount of the IL were found to strongly affect the porosity of the carbon aerogel. Interestingly, mixing with 10% [BMIm][BF<sub>4</sub>] not only increases the surface area from 371 to 559 m<sup>2</sup> g<sup>-1</sup>, but also introduces additional mesopores (of pore size around 7.0 nm) compared with the original carbon aerogel without an IL template (Figure 21).<sup>108</sup> The porous structures and surface areas of the IL-templated carbon aerogels can be further developed by KOH activation of the as-synthesized dry resorcinol–formaldehyde gel.<sup>107</sup> Use of a combination of phenol and formaldehyde as precursors and [BMIm][PF<sub>6</sub>] as a pore generator leads to the formation of macroporous carbon.<sup>109</sup>

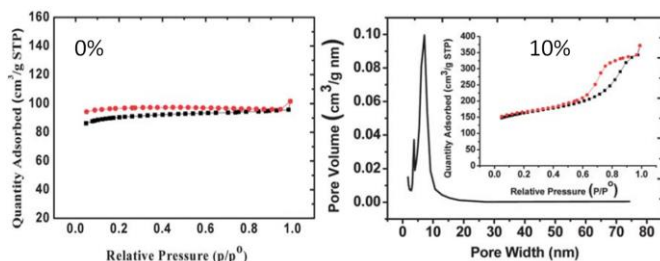


**Figure 21** N<sub>2</sub> adsorption–desorption isotherms of carbon aerogels with variable amounts of IL ([BMIm][BF<sub>4</sub>]). [Adapted from Ref. 108.]

## 4. Synthesis of metal-doped carbons from ionic liquids

ILs in the presence of metal salts or metal-containing ILs can be directly carbonized to carbon materials supporting metal nanoparticles; this approach has the following advantages. First, the presence of metal salts during carbonization greatly improves the graphitic structure of the obtained carbon materials,<sup>69, 114</sup> as observed in the case of catalytic growth of CNTs from metal particles.<sup>115</sup> Secondly, mesopores can be developed by migration and aggregation of metal nanoparticles during carbonization.<sup>116</sup> Thirdly, the resultant metal-particle-doped carbon materials have potential applications in areas such electrocatalysis and chemical catalysis. The carbon materials containing metal particles synthesized from ILs can be classified into two types, according to the supported metal nanoparticles: one is carbon materials doped with transition metals such as Fe,<sup>69, 113, 117</sup> Co,<sup>118</sup> and Ni,<sup>118</sup> and the other is carbon materials doped with precious metals such Au, Pd, and Pt.<sup>119-121</sup> It should be noted that carbon materials containing magnetic metal particles such as Fe can be easily transferred and separated by applying a magnetic field.<sup>117</sup>

We first consider the case of transition-metal nanoparticles supported on carbon materials. Direct carbonization of IL monomers containing cross-linking groups, or their corresponding poly-ILs, in the presence of FeCl<sub>2</sub> was reported to yield highly conductive, mesoporous, graphitic carbon nanostructures.<sup>69</sup> As shown in Figure 22, the threshold temperature for producing a large surface area is 900 °C. Above 900 °C, the nitrogen sorption isotherms exhibit a type H2 hysteresis loop, with a pronounced desorption step. This indicates delayed capillary evaporation and the presence of constrictions in the mesoporous structure (cage-like or bottle-like pores), and a broad pore size distribution. Moreover, HRTEM shows that all these textures are made up of stacked graphene sheets with a spacing of 0.338 nm (Figure 22B), very close to the interplanar spacing in graphite,<sup>94</sup> confirming that the lamellar-like graphitic nanostructures survived the HCl etching process. The pyrolysis of block copolymers comprising a hydrophilic poly-IL segment in the presence of metal salts such as FeCl<sub>2</sub>·4H<sub>2</sub>O and CrCl<sub>3</sub>·6H<sub>2</sub>O enables the preparation of mesoporous carbon nanomaterials with comparatively well-developed graphitic structures.<sup>122</sup> Metal-containing ILs such as [BMIm][FeCl<sub>4</sub>] can be directly carbonized to mesoporous carbon/iron carbide hybrids by confining the IL precursor within a monolithic mesoporous silica matrix. The high fractions of Fe<sub>3</sub>C and γ-Fe<sub>2</sub>O<sub>3</sub> render these materials magnetically responsive for facile separation, and they have, from the silica exotemplate, high surface areas of up to 800 m<sup>2</sup> g<sup>-1</sup>.<sup>117</sup> Other transition metals such as Co and Ni can also be deliberately added during carbonization of IL precursors.<sup>118</sup> The content and type of transition metal were found to affect the sp<sup>2</sup> carbon network and nitrogen configuration slightly, thus influencing the final oxygen reduction reaction (ORR) activity.

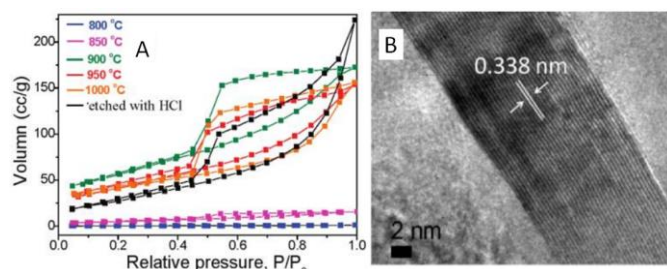


**Figure 22** (A) nitrogen sorption isotherms of carbons prepared by carbonization of IL monomers at different temperatures in presence of  $\text{FeCl}_2 \cdot 4\text{H}_2\text{O}$  and (B) HRTEM images of carbon pyrolyzed at 1000 °C after HCl etching. [Reprinted with permission from Ref. 69, copyright 2010 American Chemical Society.]

Binary and ternary metal nitride@nitrogen-doped carbon composites were obtained by template-free, one-pot carbonization of mixtures containing ILs and the corresponding metal precursors,  $\text{TiCl}_4$  or  $\text{VOCl}_3$ ; the ILs act as both carbon and nitrogen sources.<sup>123</sup> The composites were produced simply by dissolving the respective metal precursors in the IL, *i.e.*, [BMP][DCA], and subsequent calcination of the mixture. The introduction of metal ions into the precursor solution results in the formation of metal nitride nanoparticles with a narrow diameter distribution of around 7 nm, which are homogeneously distributed in a nitrogen-doped carbon matrix. Not only the amount of metal nitride in the composite but also the metal ratio in the ternary compound can be easily controlled by varying the metal precursor concentration in the starting solution. Nitrogen sorption measurements show that the composites have accessible micropores with surface areas of 350 and 550  $\text{m}^2 \text{g}^{-1}$  for  $\text{TiN@N-dC}$  and  $\text{VN@N-dC}$ , respectively. The introduction of simple salts, *i.e.*, cesium and zinc acetate, as porogens, into the IL mixture increases the surface area to 2400  $\text{m}^2 \text{g}^{-1}$ .<sup>124</sup>

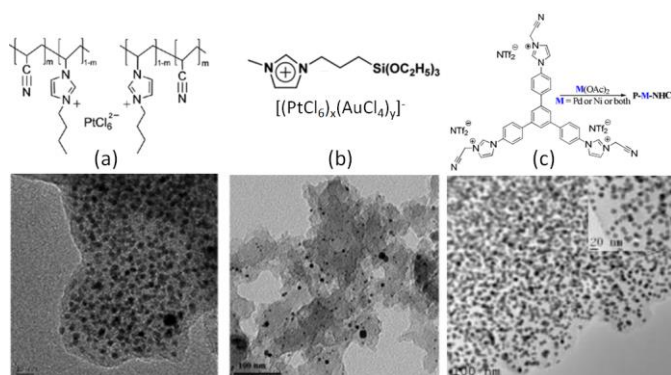


**Figure 23** Typical IL-based precursors for one-pot synthesis of precious-metal nanoparticles supported by carbon materials. [Panel (a) adapted from Ref. 119. Panel (b) adapted from Ref. 120. Panel (c) reprinted with permission from Ref. 121, copyright 2013 American Chemical Society.]

In the case of precious-metal nanoparticles supported by carbon materials, we only discuss the one-pot synthesis from composite ILs;<sup>119–121</sup> the post deposition of metal nanoparticles on as-synthesized IL-based carbons will not be considered.<sup>68, 100</sup> Typical IL-based metal-containing precursors are shown in Figure 23. Clearly, most of the structures feature metal-containing anions. For example, anion exchange between a

polymerizable IL, *i.e.*, poly(1-butyl-3-vinylimidazolium bromide-*co*-acrylonitrile), and a Pt precursor ( $\text{H}_2\text{PtCl}_6$ ), and direct carbonization of the obtained sample (Figure 23a) produced nitrogen-doped carbon–Pt nanohybrids. It can be clearly seen from the TEM image that the produced carbon material had a high loading of well-dispersed Pt nanoparticles, with a relatively narrow size distribution and an average size of ca. 3.5 nm. This hybrid showed high catalytic activity and stability in the electrocatalytic oxidation of methanol.<sup>119</sup> Pt–Au nanoparticle–carbon was obtained *via* carbonization of triethoxysilane-derived ILs containing  $[\text{PtCl}_6]_x[\text{AuCl}_4]_y$  anions (Figure 23b). The triethoxysilane group was transferred *in situ* into a silica template, and the exchanged anions provided Pt and Au sources. The resultant Pt–C hybrids show high electroactivity in methanol oxidation in an acidic medium, and  $\text{Pt}_4\text{Au}_1\text{-C}$  shows high activity in 4-nitrophenol reduction.<sup>120</sup> Analogously, Pd-nanoparticle-supported porous nitrogen-doped carbon was prepared by direct carbonization of an IL-like salt (Figure 23c); the product gave a catalytic performance even higher than that of a typical  $\text{Pd}^{2+}$  homogeneous catalyst.<sup>121</sup> Although all the IL-based precursors give a homogeneous distribution of metal nanoparticles in the carbon materials, the one-pot method is not cost effective, because it requires large amounts of precious-metal salts for anion exchange.

## 5. Introducing pores into IL-derived carbons

Although IL-derived carbons have attractive features such as high nitrogen contents and graphitic structures, most of the directly carbonized samples are unsuitable for immediate applications, mainly because of non-porous structures or low surface areas. It is therefore desirable to maximize the potential applications of IL-derived carbons by introducing adequate porosity into the IL-derived carbon structure. As expected, high porosity facilitates mass transport and diffusion, providing abundant active sites for efficient processes such as chemical catalysis and electrocatalysis.

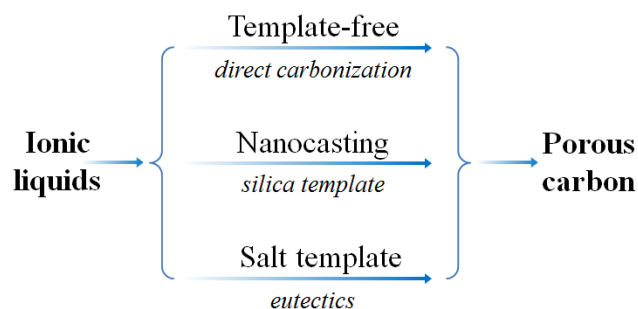


**Figure 24** General routes for preparation of porous carbon from IL precursors.

### 5.1. Template-free method

As shown in Figure 24, several methods have been used to produce porous carbons from ILs. Among them, direct carbonization of the precursor, without additional templates and complex procedures, *i.e.*, the template-free method, is the simplest, but it is challenging, mainly because of the following two issues. First, most organic compounds, because of their low thermal stabilities, are completely evaporated/decomposed to volatile products during carbonization; secondly, even for those precursors that can survive severe carbonization conditions, pores are generally unavailable because of the lack of suitable and stable self-sacrificial porogens.<sup>25, 93</sup>

Identification of appropriate carbon precursors, which could simultaneously address these two issues, is the key to guaranteeing successful fabrication of porous carbons *via* a template-free approach. The pioneering work by Dai *et al.* showed that a series of cyano-containing imidazolium ILs, if combined with bulky anions such as [NTf<sub>2</sub>] or bis(perfluoroethylsulfonyl)imide ([BETI]), could give rise to porous carbon *via* direct carbonization.<sup>25</sup> For instance, simply replacing [NTf<sub>2</sub>] by chloride for a fixed cation [BCNIm] results in a decrease in the surface area from 640 to 15.5 m<sup>2</sup> g<sup>-1</sup>, nearly complete loss of porosity. The cationic structure was found to affect the textural properties of the resulting carbon slightly. As shown in Figure 25a, although carbon derived from [BCNIm][NTf<sub>2</sub>] with bisnitrile-functionalized cations was strictly microporous (type I isotherm), [MCNIm][NTf<sub>2</sub>], containing a single-nitrile-bearing cation, produced carbon with a typical type IV isotherm, with an associated H2-type hysteresis loop, indicating the presence of significant mesoporosity.<sup>125</sup> The generation of mesoporosity with a surface area of up to 780 m<sup>2</sup> g<sup>-1</sup>, without a templating phase, is remarkable; the non-cross-linked parts such as bulky anions are believed to act as self-templates during carbonization.<sup>25</sup> Poly-ILs (Figure 7a) derived from such IL monomers containing both nitrile-bearing cations and bulky anions also give rise to micro/mesoporous nitrogen-doped carbons, even at unexpectedly low temperatures (ca. 500 °C); the polymer backbone acts as the carbon precursor as well as the nitrogen source, and the counter-ion acts as a molecular template.<sup>126</sup>

The mesoporous structures of specific nitrile-containing ILs with bulky anions can be further developed by careful design of the cationic component.<sup>127, 128</sup> For example, modification of the cationic structure using a bisimidazolium motif (Figure 26c) enabled synthesis of hierarchical nanoporous carbons *via* direct carbonization. Not only the length, but also the type, of the linker located between the two symmetric imidazolium cores was found to have a profound influence on the final porous structure. As shown in Figure 26c and Table 2, when the number of methylene spacers is above four, a longer linker greatly decreases the surface area, from 870 m<sup>2</sup> g<sup>-1</sup> for [BBI][NTf<sub>2</sub>] to 588 m<sup>2</sup> g<sup>-1</sup> for [NBI][NTf<sub>2</sub>], mainly because of depression of micropore formation. Replacing the methylene spacer by a *p*-xylyl group yields a porous carbon with very high microporosity. Interestingly, for the IL [EBI][NTf<sub>2</sub>], with a very short methylene spacer, the resultant carbon exhibits a high surface area of 854 m<sup>2</sup> g<sup>-1</sup> and a very low microporosity ( $S_{\text{mic}} = 269 \text{ m}^2 \text{ g}^{-1}$ ), suggesting a mainly mesoporous structure. Changing the anion of [EBI][NTf<sub>2</sub>] from [NTf<sub>2</sub>] to a more bulky one, *i.e.*, [BETI], can further improve the surface areas up to 1300 m<sup>2</sup> g<sup>-1</sup>; however, this is mainly the result of micropore development.<sup>127</sup>

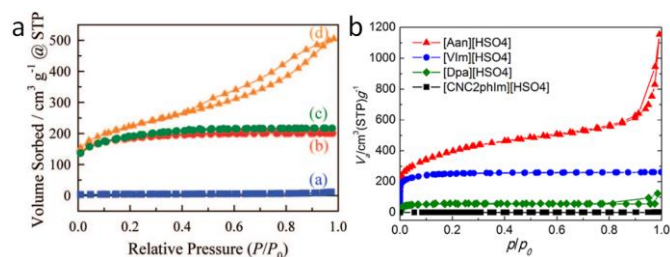


**Figure 25** Nitrogen sorption isotherms of carbons from (left) cyano/nitrile-containing aprotic ILs (a, [BCNIm][Cl]; b, [BCNIm][NTf<sub>2</sub>]; c, [BCNIm][BETI]; and d, [MCNIm][NTf<sub>2</sub>]) and (right) from PILs and salts. [Panel a reprinted with permission from Ref. 25, copyright 2010 American Chemical Society. Panel (b) reprinted with permission from Ref. 93, copyright 2014 American Chemical Society.]

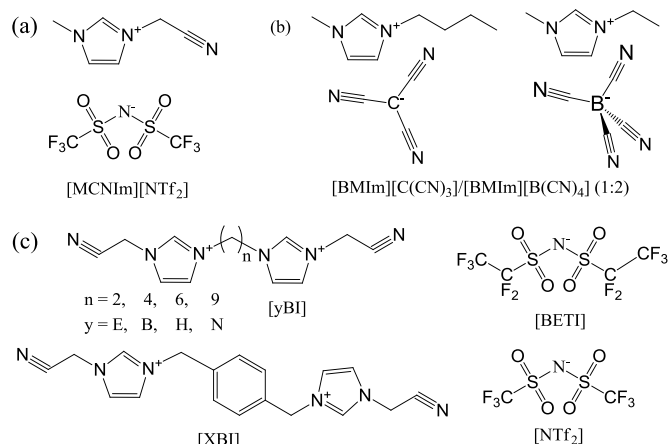


**Figure 26** Structures of ILs or IL mixtures that can generate mesoporous carbons.

**Table 2.** Porosities of carbons derived from ILs containing bisimidazolium motif *via* template-free method.

IL	$S_{\text{BET}}$ [m <sup>2</sup> g <sup>-1</sup> ]	$V_{\text{tot}}$ [cm <sup>3</sup> g <sup>-1</sup> ]	$S_{\text{mic}}$ [m <sup>2</sup> g <sup>-1</sup> ]	$V_{\text{mic}}$ [cm <sup>3</sup> g <sup>-1</sup> ]
[EBI][NTf <sub>2</sub> ]	854	1.00	269	0.12
[EBI][BETI]	1277	1.28	757	0.34
[BBI][NTf <sub>2</sub> ]	870	0.52	716	0.33
[HBI][NTf <sub>2</sub> ]	643	0.33	601	0.28
[NBI][NTf <sub>2</sub> ]	588	0.34	520	0.24
[XBI][NTf <sub>2</sub> ]	706	0.33	686	0.32

<sup>a</sup>Data from ref. <sup>127</sup>. For structures of ILs, please refer to Figure 26c.

In addition, certain PILs/PSs can directly yield porous carbons with porous structures, depending on the precursor structures (Figure 25b).<sup>91, 93</sup> In particular, [Aan][HSO<sub>4</sub>]-based carbon has a surface area of 1380 m<sup>2</sup> g<sup>-1</sup>. As shown in Figure 25b, its nitrogen sorption shows a typical type I isotherm with two sharp uptakes at low ( $P/P_0 < 0.15$ ) and high ( $P/P_0 < 0.9$ ) relative pressures, respectively, indicating that it is a microporous material with some small macropores. A mixture of [BIMIm][C(CN)<sub>3</sub>]/[BIMIm][B(CN)<sub>4</sub>] (1:2) was also reported to give rise to porous carbon with slit-like pores and a specific surface area exceeding 500 m<sup>2</sup> g<sup>-1</sup> *via* direct carbonization (Figure 26b).<sup>41</sup> Moreover, copolyolysis of IL monomers and IL homopolymers or block copolymers with metal salts enables the preparation of mesoporous carbon nanomaterials.<sup>69, 122</sup> In this case, the mesopores are thought to develop by migration and aggregation of metal nanoparticles during carbonization.<sup>116</sup> Considering that porous carbons generally can only be obtained *via* a nanocasting method or activation, the generation of porosity, especially mesoporosity, from certain ILs, based on a template-free method, is significant and should be of wide interest.

## 5.2. Nanocasting method, mainly based on silica template

Although certain ILs give porous carbons *via* template-free carbonization, as noted above, most IL-derived carbons have either no pores or very low surface areas in the absence of templates.<sup>26, 35, 118</sup> In particular, cyano-containing ILs, because of the intrinsically high nitrogen contents, high conductivities, and graphitic structures of the resultant carbons, have been intensively investigated as carbonaceous precursors. However, the materials produced by direct carbonization have small or negligible surface areas, probably because of strong cross-linking polymerization and condensation. For example, the carbons obtained at 800 °C from [EMIm][DCA], [EMIm][C(CN)<sub>3</sub>], and [EMIm][B(CN)<sub>4</sub>] have surface areas as low as 3.41,<sup>118</sup> 14<sup>41</sup> or 3.8,<sup>31</sup> and 65 m<sup>2</sup> g<sup>-1</sup>,<sup>41</sup> respectively. In most cases, therefore, sophisticated nanocasting techniques based on hard templates are needed to prepare porous carbons from ILs; the morphology of the obtained material can be controlled by manipulating the template structure, as in the case of traditional precursors. Unlike traditional precursors such as sucrose,<sup>129</sup> furfuryl alcohol,<sup>130, 131</sup> and polyacrylonitrile,<sup>132</sup> ILs can be directly carbonized at ambient pressure without any acidic or metal catalysts for prepolymerization prior to carbonization. This favors their easy incorporation into the voids of (inorganic or polymeric) templates to produce advanced nanoporous carbon materials. Other advantages of a liquid state and high thermostability, as well as the good energetic interactions between most ILs and inorganic surfaces,<sup>35, 46, 133</sup> may also facilitate homogeneous coverage of ILs on the template surface, without the necessity of using additional solvents or pressure. It has been reported that favorable interactions of liquid salts with polar inorganic structures enables the synthesis of titania nanocrystals<sup>134</sup> or hollow microspheres,<sup>135</sup> mesoporous silica,<sup>136</sup> photoluminescent EuF<sub>3</sub> nanospheres,<sup>137</sup> and other functional nanostructures.<sup>46</sup>

The facile synthesis of nitrogen-doped mesoporous carbons was achieved *via* direct infiltration of ordered mesoporous silica (SBA-15) with a pure IL, *i.e.*, [3MBP][DCA], followed by carbonization and template removal. The TEM in Figure 27 shows good replication of the two-dimensional pore structure of the SBA-15 template in the nitrogen-doped carbon. Nitrogen sorption measurements revealed that this replica is indeed mesoporous, with a maximum pore size of 3.8 nm (compared with 4.2 nm for the SBA-15 template) and a specific surface area of 906 m<sup>2</sup> g<sup>-1</sup> (compared with 844 m<sup>2</sup> g<sup>-1</sup> for the SBA-15 template).<sup>26</sup> SBA-15 was then used with other ILs for the synthesis of mesoporous carbon materials for various potential applications.<sup>138-142</sup>

Although an SBA-15 template, which has periodically ordered hexagonal mesopores, can produce ordered porous carbons from ILs, the preparation of such ordered silica templates involves complex steps and is therefore expensive and time consuming.<sup>143, 144</sup> Alternatively, disordered, but low-cost and commercially available, colloidal silica materials such as LUDOX®HS-40 (12 nm silica nanoparticles) are ideal templates for use in nanocasting approaches to the generation of nanostructured, mesoporous carbons from IL precursors.<sup>26, 27, 34, 35, 145-148</sup> For example, cocarbonization of [EMIm][DCA] with nucleobases in the presence of LUDOX®HS-40 yielded highly nitrogen-doped carbons with high surface areas and large pore volumes of up to 1553 m<sup>2</sup> g<sup>-1</sup> and 2.58 cm<sup>3</sup> g<sup>-1</sup>, respectively.<sup>27</sup> In contrast, the carbon obtained from a single IL precursor such as [BMP][DCA] has a much lower surface area, 320 m<sup>2</sup> g<sup>-1</sup>,<sup>145</sup> suggesting that the porosity of the templated carbon derived from ILs depends on the precursor structure.

A combination of a sol-gel process and use of an IL appended with a prolonged aliphatic chain ([NHP][DCA]) was used to synthesize mesoporous composite materials containing nitrogen-doped carbon and silica, by controlled condensation and subsequent thermal treatment.<sup>149</sup> [NHP][DCA] played a bifunctional role during the synthesis: as an active cationic surfactant capable of inducing mesostructures, and as a precursor for advanced chemical modifications of the targeted materials. The concentration of [NHP][DCA] strongly affected the porosity and micrographs of the resultant carbons. With increasing concentration from 1.2 to 1.6 mmol, the surface area decreased from 994 to 717 m<sup>2</sup> g<sup>-1</sup>, with bimodality appearing at high concentrations. The composite materials consisted of submicron-sized particles, and the mesopores tended to be more ordered when higher concentrations of [NHP][DCA] were used. However, after removal of the silica from the high-concentration composite, the obtained pure carbonaceous component did not exhibit any specific order and the surface area decreased to 467 m<sup>2</sup> g<sup>-1</sup>. The collapse of the structure could be caused by mutual stabilization of the silica and nitrogen-doped carbon components.<sup>149</sup> ILs with long aliphatic chains, such as 1-hexadecyl-3-methylimidazolium bromide ([C<sub>16</sub>MIm][Br]), can be used as both the carbon source and structure-directing agent, in combination with an *in situ* sol-gel process and simple one-step assembly.<sup>150</sup> Partially graphitic, mesoporous carbon with a Brunauer-Emmett-Teller (BET) surface area of 372 m<sup>2</sup> g<sup>-1</sup> and mesopore volume of 0.61 cm<sup>3</sup> g<sup>-1</sup> was obtained. The nitrogen in the IL precursor was incorporated into the carbon framework, resulting in a content of 3.2 wt%.<sup>150</sup> Impregnation of monodisperse silica spheres with [C<sub>n</sub>MIm][Br]-based ILs without cross-linkable groups, gave nitrogen-doped, uniform HCSs, as a result of interactions between the ILs and the silica sphere surfaces.<sup>47</sup> The morphology of the HCSs, including the size and shell thickness,

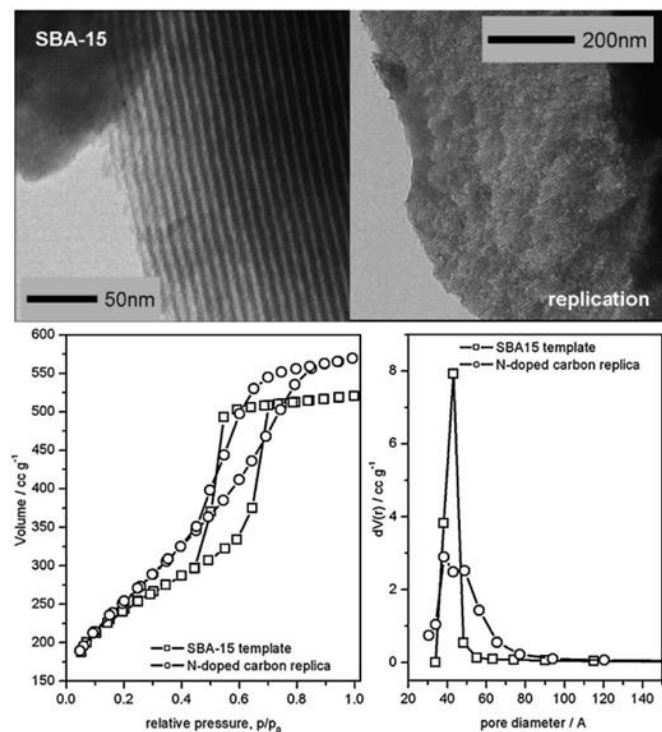


**Figure 27** TEM images and nitrogen sorption isotherms of SBA-15 template and nitrogen-doped carbon replica from [3MBP][DCA]. [Reprinted with permission from Ref. 26, copyright 2010 Wiley.]

can be adjusted by controlling the IL/silica sphere molar ratio. Considering that these ILs are generally viewed as non-carbonizable precursors, because of the lack of stable polymeric intermediates or formation of volatile decomposition intermediates, the interactions between the IL precursors and silica template are expected to be the key to inducing a carbon yield from the IL precursor and forming carbon spheres.<sup>43</sup> It should be noted that this method is simpler than that using polymerizable IL monomers mentioned above.<sup>64, 66, 67</sup> In addition, through simple coating of ILs on the surfaces of silica nanospheres and an annealing process, nitrogen-doped carbon nanobubbles<sup>52</sup> or HCSs<sup>47</sup> can be easily fabricated. The obtained nanobubbles have multiscale nanopores and abundant few-layer graphitic zones in the thin shells, which exhibit excellent ion-storage capabilities and enhanced cyclic stability in high-rate kinetic-dominated processes for LIBs.<sup>52</sup>

The nanocasting method can be extended to other hard templates such as porous alumina membranes,<sup>35</sup> silica monoliths,<sup>35</sup> and magadiite.<sup>114</sup> In particular, in the presence of magadiite as a layered template, high-surface-area graphenetype nanosheets were obtained in high yields from imidazolium-based eutectic ILs containing certain transition-metal salts as carbon precursors.<sup>114</sup> The proposed mechanism involves the intercalation of the ILs within the magadiite layers; intercalation proceeds until exfoliation of the silicate into few-layer organic-inorganic nanocomposites, carbonization, and magadiite dissolution. This facile method may enable the synthesis of dispersible carbon nanosheets from two-dimensional templates for energy-storage and -conversion devices.

### 5.3. Salt templates

The widely used silica-based templating method generally requires hazardous chemicals for template removal, so it is time and energy consuming. To overcome these drawbacks, Antonietti *et al.* recently developed a new technique called salt templating for preparing porous carbons using various low-melting point eutectic salt mixtures (Figure 28).<sup>42, 124, 151-154</sup> The overall procedure for salt templating is very simple (Figure 28a).<sup>151</sup> An IL (precursor) is mixed with a non-carbonizable inorganic eutectic salt (template), forming a glassy beige solid, which is condensed and scaffolded in the presence of the molten salt at elevated temperatures. After carbonization in a nitrogen atmosphere and simple aqueous removal of the salt porogen, highly porous nitrogen- or nitrogen/boron-doped carbons are obtained. The porogen can be recovered for further use, which results in a closed-loop process including salt recycling. The following two factors are believed to facilitate the homogeneity of the precursor mixtures and the generation of highly porous heteroatom-doped carbons. First, the strong coulombic interactions exist between the ILs and salt molecules, which are proven by the exothermicity of the process of mixing of the precursor and template prior to carbonization. Secondly, the melting points of the eutectics are below the onset temperature of cross-linking of the IL units.

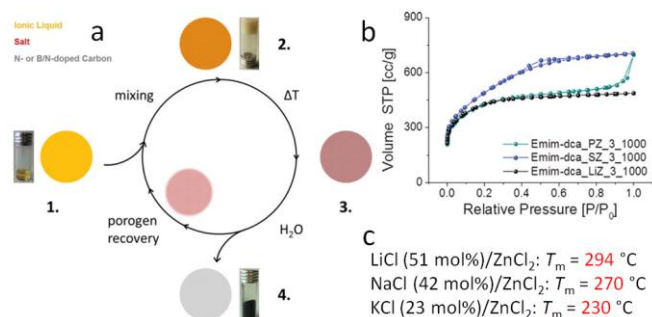


**Figure 28** (a) Diagram of salt-templating approach, (b) nitrogen sorption isotherms of [EMIm][DCA]-derived carbons templated with LiZ (LiCl–ZnCl<sub>2</sub>), SZ (NaCl–ZnCl<sub>2</sub>), and PZ (KCl–ZnCl<sub>2</sub>), and (c) compositions and melting points of eutectic-based salt templates. [Reprinted with permission from Ref. 151, copyright 2013 Wiley.]

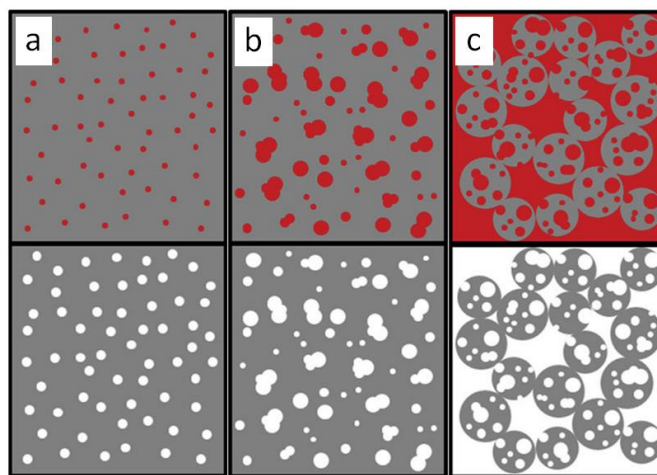


**Figure 29** Schematic representation of pore formation for carbons templated with LiZ (a), SZ (b), and PZ (c) at equal mass ratios. The upper image depicts the carbon (grey)/salt (red) composite, and the lower images show carbon after washing. [Reprinted with permission from Ref. 151, copyright 2013 Wiley.]

The pore morphology and porosity of the resultant carbon were shown to depend solely on the nature of the templating salt, and not on the IL. The nitrogen sorption isotherms of [EMIm][DCA]-based carbons are shown in Figure 28b as an example. In the case of eutectic LiZ (LiCl–ZnCl<sub>2</sub>), the isotherm is type I, which implies that the carbon has a solely microporous structure, *i.e.*, the salt presumably acts as a molecular template, either forming ion pairs or small salt clusters of minimal free energy (Figure 29a). For carbons templated with SZ (NaCl–ZnCl<sub>2</sub>), the sorption isotherms of the materials show a further uptake in the medium relative pressure region, as well as a small hysteresis (Figure 28b), reflecting a substantial contribution from additional supermicropores and small mesopores. This could be attributed to the lower melting point of SZ and larger salt clusters, resulting from the onset of phase demixing in the later stages of condensation, giving structures in the 4 nm range, which now act as a template (Figure 29b). Finally, for materials templated with PZ (KCl–ZnCl<sub>2</sub>) which has the lowest melting point, additional uptake in the high relative pressure region is observed (Figure 28b). This is typical of macroporous materials. Particle formation is

ascribed to more pronounced demixing in earlier phases of the cross-linking reaction, resulting in a continuous salt phase (Figure 29c), therefore interstitial voids between the micro- and meso-porous particles become visible. Based on a combination of the effects of salt concentration on pore formation, highly micro-, meso-, and macro-porous carbon materials can be easily obtained, depending on the salt nature and amount. The resultant carbon can be tuned to be highly porous, with surface areas up to  $2000 \text{ m}^2 \text{ g}^{-1}$ , even higher than those of zeolites or activated carbons, and approaching the value for single-layer graphene.<sup>151</sup> This newly developed salt-templating method has been used to prepare highly porous carbon/metal nitride nanocomposites,<sup>124</sup> and nitrogen and sulfur codoped hierarchically porous carbons from non-carbonizable ILs.<sup>50</sup> For example, by calcining a mixture of an IL ([Emim][DCA]) as both the nitrogen and carbon sources, a metal precursor ( $\text{VOCl}_3$  or  $\text{NH}_4\text{VO}_3$ ), and simple salts (cesium and zinc acetate) as porogens, vanadium nitride nanoparticles embedded in a porous nitrogen-doped carbon matrix were prepared; the surface area, pore volume, pore size, and nanoparticle size can be tuned based on the amount and nature of the porogen salt.<sup>124</sup>

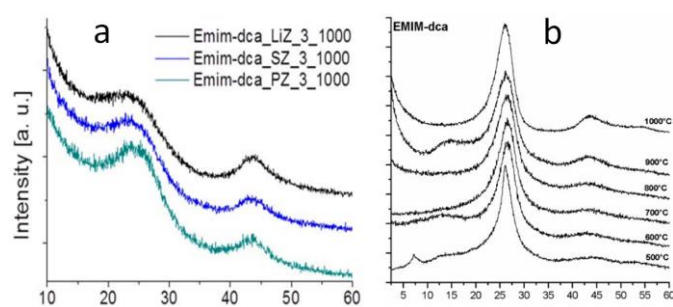


**Figure 30** XRD patterns of carbon derived from [EMIm][DCA] (a) with or (b) without salt template. [Panel a reprinted with permission from Ref. 151, copyright 2013 Wiley. Panel b reprinted with permission from Ref. 26, copyright 2010 Wiley.]

However, compared with the carbon obtained *via* direct carbonization of [EMIm][DCA], the salt-templating approach leads to a slight depression of the chemical functionality and structure. For example, the highest nitrogen content from [Emim][DCA]-based carbons is 6.1 wt% at  $1000^\circ\text{C}$ ,<sup>151</sup> which is lower than the value of 10.4 wt% obtained in the absence of a template at the same temperature.<sup>26</sup> In addition, instead of the well-developed and sharp stacking 002 peak observed for the directly carbonized carbon, the salt-templated carbon exhibits a broad, lower-shifted peak (Figure 30), indicating that the graphitic structure becomes amorphous.

#### 5.4. Other methods

IL-derived carbons prepared using hard templates such as mesoporous silica still suffer from low surface areas. Metal-organic frameworks (MOFs), because of their exceptionally large surface areas and controlled pore textures, have potential for use as templates for the synthesis of nanoporous carbon materials.<sup>155</sup> Recently, Xu *et al.* demonstrated a simple method for fabricating high-surface-area, uniformly nitrogen- and boron-nitrogen-doped nanoporous carbons by impregnation of cyano-containing ILs within a MOF to produce a precursor/template composite, followed by carbonization (Figure 31).<sup>156</sup> The obtained heteroatom-doped microporous

carbons have narrow pore size distributions and high surface areas of up to  $2397 \text{ m}^2 \text{ g}^{-1}$ .



**Figure 31** Schematic illustration of procedure for nanoporous carbon synthesis from MOF and ILs. [Reproduced from Ref. 156.]

Incorporation of phosphorus-containing additives such as tetraalkylphosphonium bromide into the [BMP][DCA] IL precursor not only yielded nitrogen- and phosphorus-codoped carbons, but also promoted the formation of porous carbons with surface areas up to  $283 \text{ m}^2 \text{ g}^{-1}$ .<sup>157</sup> The properties of the alkyl chains and the additive concentration both determine the achieved surface area, indicating a templating effect of the phosphonium salts. In addition, Watanabe *et al.* found that blending common PILs/PSs such as [Dema][HSO<sub>4</sub>] with a non-carbonaceous [H<sub>2</sub>PO<sub>4</sub>]-containing PIL with only 12 wt% doping greatly increased the surface area, from 690 to  $1355 \text{ m}^2 \text{ g}^{-1}$ ;<sup>91</sup> this result is very similar to the activation effect of phosphoric acid.<sup>158-160</sup>

## 6. Applications of ionic-liquid-derived carbons

The use of IL precursors for carbon formation has developed rapidly in the past five years, and the properties of the obtained carbon materials make them highly promising for potential applications in diverse areas such as energy storage and conversion,<sup>27, 145</sup> gas storage,<sup>32</sup> adsorption,<sup>126</sup> sensing,<sup>56</sup> and catalysis.<sup>146</sup> However, it should be noted that the target applications depend strongly on the carbon structure, and therefore on the original precursor. For example, DES-derived carbons with highly microporous structures are mainly used as solid adsorbents for CO<sub>2</sub> capture or as electrode materials for supercapacitors, whereas [EMIm][DCA]-derived porous carbons with very high nitrogen contents are expected to be efficient electrocatalysts. More specifically, the applications can be divided into five main classes, *i.e.*, electrocatalysis, LIBs, supercapacitors, CO<sub>2</sub> capture, and chemical catalysis; these are discussed separately.

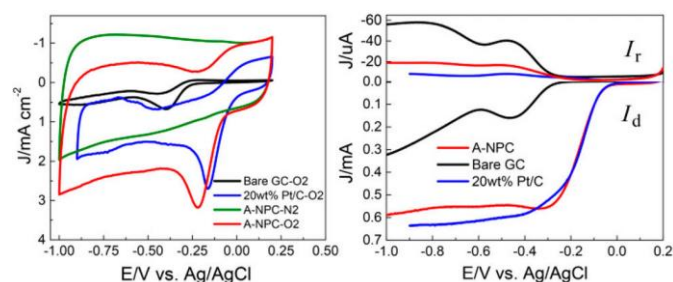


**Figure 32** CV and RRDE results for bare, glassy carbon, A-NPC,

and commercial 20 wt% Pt/C in O<sub>2</sub>-saturated 0.1 M KOH solution. [Reprinted with permission from Ref. 93, copyright 2014 American Chemical Society.]

### 6.1. Electrocatalysis

A highly attractive application is electrocatalysis, *e.g.*, in the ORR. The ORR is currently the technological bottleneck for the industrial development of fuel cells.<sup>161</sup> Pt-based materials have long been investigated, as they are the most efficient catalysts for the ORR.<sup>162</sup> However, the scarcity, high cost, sluggish ORR process, intolerance to fuel cross-over, and poor long-term stabilities of Pt-based catalysts are major obstacles. Nitrogen-doped carbon materials were recently shown to be efficient ORR electrocatalysts;<sup>28, 163-165</sup> they exhibit significant ORR performances, and have long-term stability and excellent resistance to cross-over effects.<sup>27, 166</sup> The highly nitrogen-doped carbons intrinsically obtained from IL precursors are therefore expected to find potential applications as metal-free electrocatalysts for the ORR.<sup>167, 168</sup> For example, *via* carbonization of nucleobases in [EMIm][DCA] in the presence of LUDOX®HS-40, mesoporous carbon materials with nitrogen contents of up to 12.0 wt% and high surface areas of up to 1553 m<sup>2</sup> g<sup>-1</sup> were obtained; they exhibited high ORR activities and durability.<sup>27</sup> The abundant mesopores in the carbons facilitate efficient diffusion/mass transfer and provide a large amount of accessible active sites for electrocatalysis. Notably, the cathodic currents in alkaline media are comparable to those of commercial Pt/C catalysts. A mechanistic analysis based on the Koutecky–Levich equation revealed a four-electron process ( $n = 4.1$ ), indicating selective reduction of oxygen to water. IL-derived nanostructured carbon materials such as nitrogen-doped hollow macroporous carbon spheres,<sup>71</sup> carbon nanobubbles,<sup>72</sup> and nitrogen- and sulfur-dual-doped porous carbons<sup>50</sup> also have high ORR activities. In particular, one of the nitrogen-doped porous carbons (A-NPC), obtained by direct carbonization of a PS, exhibited excellent electrocatalytic activity in the ORR, as shown by cyclic voltammetry (CV) and rotating ring–disk electrode (RRDE) measurements (Figure 32). A-NPC has an onset potential and half-wave potential very close to those of commercial Pt/C. The calculated peroxide yield was <15%, and the average electron-transfer number ( $n$ ) was >3.7.<sup>93</sup> Clearly, the ORR performance of this catalyst is much better than most of those reported for carbon-based catalysts that require special templates and complicated synthetic steps,<sup>165, 169</sup> probably because of its high surface area (1380 m<sup>2</sup> g<sup>-1</sup>), high content of pyridinic nitrogen, and possible synergistic activation by sulfur and nitrogen dual doping.<sup>169</sup> In addition, instead of water as the main product, as observed for most IL-derived carbon electrocatalysts obtained at 1000 °C, a pure two-electron reduction process from oxygen to H<sub>2</sub>O<sub>2</sub>, was achieved using nitrogen-doped carbon synthesized by silica-templated carbonization of a [DCA]-based IL at a relatively low temperature (800 °C).<sup>145</sup> The obtained porous carbon has a very high nitrogen content, 14.2 wt%, as determined by XPS, and has higher catalytic activity in the ORR than commercial carbon (Vulcan XC 72R), even in an acidic medium. The electron-transfer number was calculated to be very close to 2, indicating a pure two-electron mechanism. This high selectivity was verified by comparison of the CVs obtained in a deoxygenated electrolyte before and after the addition of H<sub>2</sub>O<sub>2</sub>. In both cases, no reduction peak or faradaic current was observed, but subsequent oxygen purging led to strong reduction currents. More recently, nitrogen-doped

carbon aerogels, made from [EMIm][DCA] using the salt-templating strategy, with surface areas up to 1800 m<sup>2</sup> g<sup>-1</sup>, were found to catalyze four-electron oxygen reduction to water. An outstanding ORR performance with a well-defined diffusion-limited region was achieved in both acidic and alkaline media, comparable to those of Pt-based commercial catalysts.<sup>154</sup>

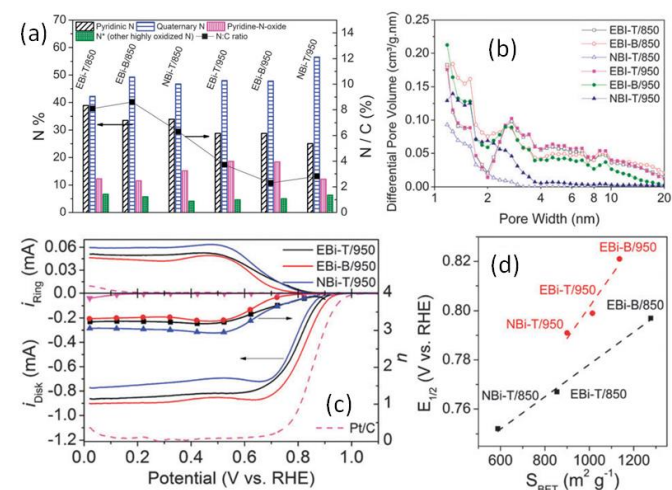


**Figure 33** (a) Nitrogen composition and (b) pore size distribution of different carbons derived from ILs containing bis[*N*-(2-cyanoethyl)imidazole] core. (c) Disk (lower part) and ring current (upper part), and number of transferred electrons ( $n$ , symbol line) of IL-derived carbon catalysts. (d) Correlation between the half-wave potentials ( $E_{1/2}$ ) and surface areas ( $S_{\text{BET}}$ ) of different carbons. [Adapted from Ref. 128.]

In order to understand if and how the porosities and pore size distributions of carbon materials affect the ORR activity, a series of nitrogen-doped carbons were obtained by direct carbonization of specific ILs containing a bis[*N*-(2-cyanoethyl)imidazole] core and bulky anions.<sup>128</sup> As shown in Figure 33a, the nitrogen contents and N/C ratios in all the catalysts are affected by the carbonization temperature rather than the type of starting material. In addition, the resultant carbons exhibit various porous structures (*i.e.*, micro- and/or meso-pores), depending on the IL structure (Figure 33b), with surface areas varying in the range 588–1277 m<sup>2</sup> g<sup>-1</sup>. These totally metal-free carbons were tested in the ORR. Interestingly, a comparison of three catalysts carbonized at the same temperature showed that the half-wave potentials ( $E_{1/2}$ ) increase monotonically with the surface areas (Figure 33d). These results indicate that the porous structure of the catalyst is a key factor in ORR activity. The pore limiting currents calculated from Koutecky–Levich plots are 5.41, 6.90, and 3.92 mA for EBi-T/950, EBi-B/950, and NBi-T/950, respectively. These results show that as well as nitrogen doping, the pore size distribution is of significance in the ORR activity of a carbon-based catalyst. Hierarchical micro- and meso-porous structures may increase the activity.

In addition to having intrinsic electrocatalytic activities, IL-derived carbon materials support metal nanoparticles. These nanoparticle-containing carbons are synthesized either by *in situ* one-pot carbonization or a post-deposition method, and they are also particularly promising electrocatalysts for reactions such as the ORR and methanol oxidization.<sup>67, 68, 119, 120, 147</sup> Most of the catalysts show activities comparable to those of benchmark commercial Pt/C catalysts, and, sometimes,

significantly increased Pt electrochemical active surface areas are observed.

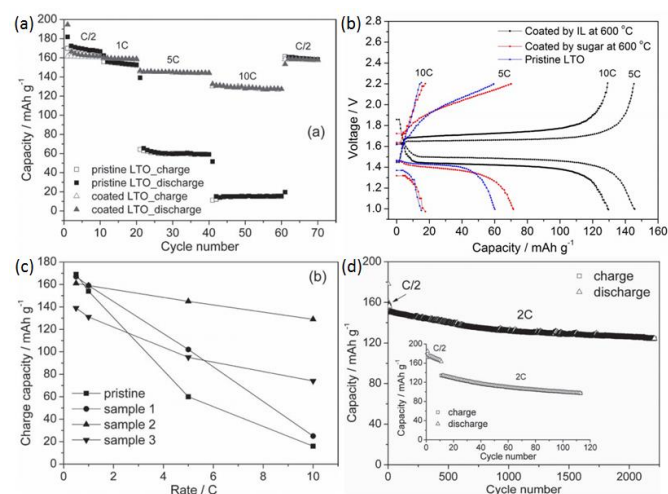


**Figure 34** (a) Discharge/charge capacities at different current rates, (b) discharge/charge curves at 5C and 10C rates, and (c) specific capacities at different current rates. Samples 1, 2, and 3 are  $\text{Li}_4\text{Ti}_5\text{O}_{12}$  coated with 3.6, 7.0, and 9.6 wt% carbon, respectively. (d) Cycling performances of pristine  $\text{Li}_4\text{Ti}_5\text{O}_{12}$  and nitrogen-doped-carbon-coated  $\text{Li}_4\text{Ti}_5\text{O}_{12}$ . [Reprinted with permission from Ref. 98, copyright 2011 Wiley.]

## 6.2. Li-ion batteries

LIBs are extensively used in portable electronic devices, because of their high energy densities and long cycling lifetimes. However, graphite, the most commonly used anode material in commercial LIBs, has a very limited Li-intercalation capacity ( $\text{LiC}_6$ ,  $372 \text{ mA h g}^{-1}$ ), which hinders its applications in transportation and large-scale energy storage. As alternatives to graphite, nanostructured porous carbons have been studied as candidates for anode materials in LIBs, because of their good chemical and thermal stabilities and high  $\text{Li}^+$ -storage capacities. In addition, the presence of heteroatoms such as nitrogen on the carbon surface can enhance the reactivity and electrical conductivity.<sup>170, 171</sup> IL-based nitrogen-doped carbons can be directly used as anode materials for LIBs.<sup>40, 52</sup> For example, IL-derived carbon nanobubbles exhibit an initial discharging capacity of more than  $3000 \text{ mA h g}^{-1}$  at a current density of  $1 \text{ A g}^{-1}$ , as well as excellent rate performances of up to  $20 \text{ A g}^{-1}$ .<sup>52</sup> Almost 100% capacity retentions were achieved for galvanostatic discharging at 1, 10, and  $20 \text{ A g}^{-1}$ , with a coulombic efficiency of nearly 100% from the fifth cycle. This superhigh capacity compared with the theoretical capacity of graphite can be explained by the presence of other Li-storage mechanisms such as storage in cavities and nanopores, in addition to the classical graphite intercalation compound mechanism.<sup>170, 171</sup> However, as observed for most porous carbons, only half of the initial discharging capacity is reversibly achieved in the charging process, suggesting a very low initial coulombic efficiency (<50%). This can be attributed to their high specific surface areas and irreversible Li insertion into special sites, such as in the vicinity of residual hydrogen atoms in carbonaceous materials, which can result in decomposition of the electrolyte and the formation of solid-electrolyte interphase (SEI) films at the electrode-electrolyte interface.<sup>170, 171, 175</sup>

In contrast to nitrogen-doped porous carbons, spinel  $\text{Li}_4\text{Ti}_5\text{O}_{12}$ , a zero-strain insertion material, gives an excellent cycling performance and a relatively high lithiation voltage plateau, at 1.54 V versus  $\text{Li}/\text{Li}^+$ , which avoids SEI formation, making it a promising anode material for large-scale, long-life, energy-storage batteries. However, its low electronic conductivity and moderate  $\text{Li}^+$  diffusion coefficient severely limit the high rate performance.<sup>176</sup> Nitrogen-doped-carbon-coated  $\text{Li}_4\text{Ti}_5\text{O}_{12}$  was obtained by carbonization of [EMIm][DCA] as a single IL precursor at  $600^\circ\text{C}$  in an Ar atmosphere.<sup>98</sup> The nitrogen-doped carbon coating derived from an IL is effective in improving the rate capability and charge/discharge properties. Compared with either pristine  $\text{Li}_4\text{Ti}_5\text{O}_{12}$ , or a solely carbon-coated sample produced using sugar as a precursor, the nitrogen-doped-carbon-coated sample has a much better rate capability at high current rates of 5C and 10C (Figure 34a and 34b). Capacities of 145 and  $129 \text{ mA h g}^{-1}$ , respectively, were achieved; the capacities of pristine  $\text{Li}_4\text{Ti}_5\text{O}_{12}$  at the same rates were 60 and  $15 \text{ mA h g}^{-1}$ , respectively. In addition, the coated samples exhibit excellent cycling performances compared with pristine  $\text{Li}_4\text{Ti}_5\text{O}_{12}$ . Even after 2200 cycles at 2C, nearly 83% of the initial capacity was retained (Figure 34d). The carbon contents of the coated samples were found to affect the specific capacity at high current rates (Figure 34c). A moderate carbon content of 7.0 wt% (sample 2) provides a thin but uniform nitrogen-doped carbon layer, which enhances the electrochemical performance. This is ascribed to significant electron transfer from the  $\text{Li}_4\text{Ti}_5\text{O}_{12}$  surface to the nitrogen-doped-carbon coating layers and the improved interfacial stability and interfacial electrical conductivity.<sup>53</sup> This IL-based carbon coating method can be extended to other cathode or anode materials such as  $\text{NiO}$  nanocrystals,<sup>173</sup> rod-like  $\text{LiFePO}_4$ ,<sup>49</sup>  $\text{Fe}_2\text{O}_3$ ,<sup>64</sup> and  $\text{Fe}_3\text{O}_4$ <sup>48</sup> nanoparticles,  $\text{TiO}_2$  nanofibers,<sup>172</sup> and  $\text{Li}_3\text{V}_2(\text{PO}_4)_3$ ,<sup>51</sup> even using non-carbonizable ILs.<sup>173</sup> Table 3 summarized the corresponding battery performance. Clearly, most of them were carbon-coated metal oxides and were explored as anode for LIBs. The resulted battery performances are somewhat related to the intrinsic capacity of the metal oxide. Although cyano/nitrile-containing aprotic ILs generally result in carbons with low surface area and low reversible capacity for LIBs, they are likely to give rise to high initial coulombic efficiency and good rate capability at high current rates.<sup>40, 98</sup> Instead of aprotic ILs, some of the above mentioned specific PILs may be also suitable organic precursors to coat metal oxide with a thin layer of N-doped carbon in the future, because the resultant carbons possess simultaneously high N content, high graphitic degree, and high conductivity. More importantly, they are easily available and low cost.

## ARTICLE

**Table 3.** Summary of Lithium-ion batteries based on different types of ILs-derived carbons.

ILs	Electrode materials	Anode/cathode	Reversible capacity	Cycling stability	Ref.
[EMIm][DCA]	N-doped carbon coated $\text{Li}_4\text{Ti}_5\text{O}_{12}$	anode	150 $\text{mAh g}^{-1}$ at 2 C 145 $\text{mAh g}^{-1}$ at 5 C 129 $\text{mAh g}^{-1}$ at 10 C	124 $\text{mAh g}^{-1}$ at 2 C after 2000 cycles	98
[EMIm][DCA]	N-doped mesoporous carbon decorated $\text{TiO}_2$ nanofibers	anode	200 $\text{mAh g}^{-1}$ at 1 C 150 $\text{mAh g}^{-1}$ at 5 C	264 $\text{mAh g}^{-1}$ at 0.1 C after 100 cycles	172
[EMIm][BF <sub>4</sub> ]	N-doped carbon coated NiO nanocrystals	anode	690 $\text{mAh g}^{-1}$ at 1 C 600 $\text{mAh g}^{-1}$ at 5 C 470 $\text{mAh g}^{-1}$ at 10 C	610 $\text{mAh g}^{-1}$ at 0.3 C after 50 cycles	173
$\text{LiC}(\text{CN})_3$	Li ion-doped carbon	anode	500 $\text{mAh g}^{-1}$ at 50 $\text{mAh g}^{-1}$	500 $\text{mAh g}^{-1}$ at 50 $\text{mAh g}^{-1}$ after 100 cycles	40
$\text{LiC}(\text{CN})_3$	Lt-600 coated mesoporous carbon	anode	620 $\text{mAh g}^{-1}$ at 50 $\text{mAh g}^{-1}$	540 $\text{mAh g}^{-1}$ at 50 $\text{mAh g}^{-1}$ after 100 cycles	40
[C8MIm][Cl]	N-doped carbon-coated $\text{Fe}_3\text{O}_4$	anode	980 $\text{mAh g}^{-1}$ at 100 $\text{mAh g}^{-1}$	880 $\text{mAh g}^{-1}$ at 100 $\text{mAh g}^{-1}$ after 100 cycles	48
[EMIm][NTf <sub>2</sub> ]	N-doped carbon-coated $\text{LiFePO}_4$	cathode	116 $\text{mAh g}^{-1}$ at 2 C 98 $\text{mAh g}^{-1}$ at 5 C 129 $\text{mAh g}^{-1}$ at 10 C	122 $\text{mAh g}^{-1}$ at 0.1 C after 30 cycles	49
[CMVIm][Br]	N-doped hollow carbon loading with $\text{Fe}_2\text{O}_3$	anode	1120 $\text{mAh g}^{-1}$ at 100 $\text{mAh g}^{-1}$	700 $\text{mAh g}^{-1}$ at 100 $\text{mAh g}^{-1}$ after 65 cycles	64
[AMIm][Br]	N, O-codoped carbon nanobubbles	anode	1394 $\text{mAh g}^{-1}$ at 1 $\text{Ah g}^{-1}$ 903 $\text{mAh g}^{-1}$ at 2 $\text{Ah g}^{-1}$ 622 $\text{mAh g}^{-1}$ at 5 $\text{Ah g}^{-1}$	1308 $\text{mAh g}^{-1}$ at 1 $\text{Ah g}^{-1}$ after 130 cycles	52
[C <sub>4</sub> mpyr][NTf <sub>2</sub> ]	Carbon-coated $\text{Li}_3\text{V}_2(\text{PO}_4)_3$	cathode	120 $\text{mAh g}^{-1}$ at 1 C 116 $\text{mAh g}^{-1}$ at 10 C 110 $\text{mAh g}^{-1}$ at 20 C	108 $\text{mAh g}^{-1}$ at 10 C after 100 cycles	51

**Table 4.** Summary of supercapacitor devices based on different types of ILs/DES-derived carbons.

ILs/DES	Electrode materials	Surface area [ $\text{m}^2 \text{g}^{-1}$ ]	electrolyte	Specific capacitance	Ref.
DES-2	Hierarchical porous MWCNT	415	2 M $\text{H}_2\text{SO}_4$	90 $\text{F g}^{-1}$ at 765 $\text{mA cm}^{-2}$	89
[EMIm][DCA]	Graphene/N-doped porous carbon composite	404	1 M $\text{H}_2\text{SO}_4$	206 $\text{F g}^{-1}$ at 0.1 $\text{A g}^{-1}$	103
DES-6	P-functionalized carbon monolith	687	2 M $\text{H}_2\text{SO}_4$	197 $\text{F g}^{-1}$ at 1.27 $\text{mA cm}^{-2}$	84
[BMIm][DCA]	N-doped mesoporous carbon	931	6 M KOH	210 $\text{F g}^{-1}$ at 1 $\text{A g}^{-1}$	142
[EBI][BETI]	N-doped hierarchical nanoporous carbon	1277	6 M KOH	Ca. 93 $\text{F g}^{-1}$ at 100 $\text{mV s}^{-1}$ Ca. 143 $\text{F g}^{-1}$ at 10 $\text{mV s}^{-1}$	127
[C16MIm][BF <sub>4</sub> ]	Hierarchically porous carbons	376	6 M KOH	247 $\text{F g}^{-1}$ at 0.5 $\text{A g}^{-1}$	105
[BMIM][Br]	Microporous carbon nanosheet	791	6 M KOH	341 $\text{F g}^{-1}$ at 5 $\text{mV s}^{-1}$ 213 $\text{F g}^{-1}$ at 0.5 $\text{A g}^{-1}$	101

**Table 5.** Summary of CO<sub>2</sub> adsorption performance for ILs/DES-derived carbons.

ILs/DES	Surface area [m <sup>2</sup> g <sup>-1</sup> ]	Heat [KJ mol <sup>-1</sup> ]	Capacity [mmol g <sup>-1</sup> ] <sup>a</sup>		Selectivity CO <sub>2</sub> /N <sub>2</sub>	Ref.
			0 °C	25 °C		
[BCNIm][NTf <sub>2</sub> ]	942	32	4.39 (19.3 wt %)	13.5wt%	N/A	<sup>32</sup>
EBI-B	1013	31.5	4.07	2.74	30	<sup>174</sup>
[Dema][HSO <sub>4</sub> ]	690	N/A	N/A	2.63	N/A	<sup>91</sup>
[EMIm][DCA]+MOF	2397	26	5.7	3.8	57	<sup>156</sup>
DES-5+ formaldehyde	666	30-31	N/A	3.3	4.3-5.7	<sup>86</sup>
DES-7+ formaldehyde	4	29.1	3.0	2.2	8.4	<sup>85</sup>
DES-8+ formaldehyde	4	N/A	3.7	2.7	N/A	<sup>87</sup>

<sup>a</sup> Capacity for CO<sub>2</sub> adsorption was measured at 1 atm.

### 6.3. Supercapacitors

Supercapacitors are attracting increasing interest because of their high power density, which are highly desirable for applications in electric vehicles. Hierarchical porous monoliths were obtained by carbonization of a composite of multiwalled CNTs (MWCNTs) and poly(furfuryl alcohol) gels formed in DES-based ILs.<sup>89</sup> The DES-assisted *in situ* condensation of furfuryl alcohol not only promoted the formation of monoliths, but also provided a carbon shell that coats every MWCNT and forms strong junctions between them (see Figure 35), resulting in a high conductivity of up to 4.8 S cm<sup>-1</sup> and a high elasticity (Young modulus, 11 MPa). The resultant carbon monolith retains 75% of the initial capacitance at a high current density of 765 mA cm<sup>-2</sup> (ca. 29 A g<sup>-1</sup>), much better than most porous carbon monoliths. The rapid electrical response of the monolithic composite was also reflected in the preservation of the rectangular CV shape at scan rates of up to 300 mV s<sup>-1</sup> (Figure 35e). It should be noted that direct processing of the monolithic carbon materials enables their direct assembly (without any further processing, such as using a binder to form pellets and/or adding carbon black to improve the electrode electrical conductivity) into supercapacitor cells (Figure 35d). Phosphate-functionalized carbon monoliths derived from DES-based ILs were reported to have high surface areas, micropores capable of accommodating protons and ions from aqueous electrolytes, and macropores that allow mass transport and accessibility to the micropores.<sup>84</sup> The phosphate functionalization of carbon materials broadens the operational voltage window of the electrode to 1.4 V,<sup>177</sup> and high energy densities of up to 13 W h kg<sup>-1</sup> were achieved.

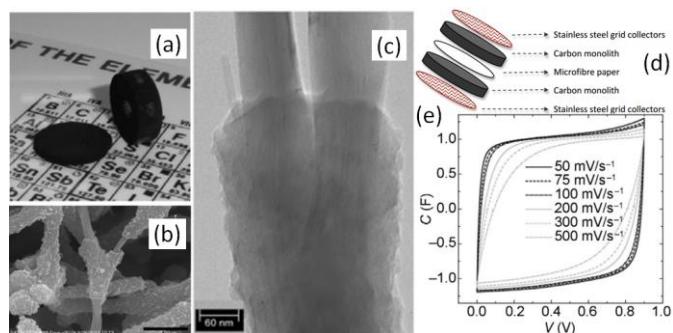


**Figure 35** (a) Photograph, (b) SEM, and (c) TEM of MWCNT-based carbon monolith, (d) schematic diagram of assembly of supercapacitor cell from carbon monolith electrodes, and (e)

CV recorded in H<sub>2</sub>SO<sub>4</sub> (2 M) at voltage scan rates between 50 and 500 mV s<sup>-1</sup>. [Reprinted with permission from Ref. 89, copyright 2011 Wiley.]

In comparison with nitrogen-free carbons obtained from DESs, the nitrogen-doped porous carbons from classic IL precursors involving nitrogen-containing cores such as imidazolium or cyano/nitrile groups are considered to be promising electrode materials for supercapacitors,<sup>127, 142</sup> because of their wettability by electrolytes, high conductivity,<sup>178</sup> and additional pseudo-capacitance, especially in acidic electrolytes,<sup>179, 180</sup> e.g., nitrogen-doped hierarchical nanoporous carbons obtained by direct, template-free carbonization of ILs with a bisimidazolium motif and bulky anion displayed capacitance values above 100 F g<sup>-1</sup> at slow scanning rates.<sup>127</sup> Carbonization of a fluidic IL, [EMIm][DCA], in an SBA-15 template at 900 °C gave a nitrogen-doped mesoporous carbon material with a high nitrogen content of 8.27 wt% and high surface area of 931 m<sup>2</sup> g<sup>-1</sup>; it has a high specific capacitance of 210 F g<sup>-1</sup> and excellent cycling stability, even after 1000 cycles at a current density of 1 A g<sup>-1</sup>.<sup>142</sup> Other nanostructured carbon materials obtained through IL-assisted synthesis have been widely explored as electrode materials for supercapacitors; in these, the ILs have one or multiple roles, e.g., as nitrogen dopants and shape-directing agents in microporous carbon nanosheets,<sup>101</sup> as nitrogen and boron sources in hierarchically porous carbons,<sup>105</sup> as templates,<sup>107</sup> and as nitrogen-rich carbon precursors in graphene/N-doped porous carbon composites.<sup>103</sup> Two-dimensional nitrogen-doped carbon sheets obtained using IL-functionalized GO as a shape-directing agent and a resorcinol-formaldehyde polymer as a carbon precursor have a microporous structure with a pore size distribution centered at 0.53 nm and a hydrophilic surface (contact angle ~69°). The assembled supercapacitor has a specific capacitance of 213 F g<sup>-1</sup> at 0.5 A g<sup>-1</sup>, excellent capacitance retention, and a long cycling life.<sup>101</sup> To give easy reference to the reader, we listed the supercapacitor performance based on different types of ILs/DES-derived carbons. As shown in Table 4, it appears that direct comparison between these carbon materials is impossible because the specific capacitances were obtained at different current density or from different methods (cyclic voltammogram or galvanostatic charge/discharge). However, the nitrogen doping structure formed during *in situ* carbonization of ILs is expected to be important to the excellent performances, which not only improves the conductivity, but also sometimes contributes pseudocapacitance to the double-layer capacitance. In addition to this point, desirable porous structure, which is essential to supercapacitor electrodes, is required to be carefully design by introducing suitable template.

#### 6.4. CO<sub>2</sub> capture

The selective capture and storage of CO<sub>2</sub> has attracted considerable attention in recent years, because CO<sub>2</sub> is a major greenhouse gas and a renewable carbon source. Nitrogen-doped porous carbons with less basic sites have emerged as promising sorbent solids for physisorption and regeneration of CO<sub>2</sub>, because of their exceptionally high surface areas, low cost, chemical inertness, and wide availability.<sup>181-188</sup> Strong binding interactions such as dipole–quadr interactions,<sup>187</sup> acid–base interactions,<sup>185</sup> and hydrogen bonding<sup>189</sup> between CO<sub>2</sub> molecules and the nitrogen-modified heterogeneous pore walls within the carbon framework significantly improve the CO<sub>2</sub> affinity of nitrogen-doped adsorbents. Nitrogen-doped porous carbons derived from ILs are therefore promising materials for CO<sub>2</sub> capture. For example, a high CO<sub>2</sub> adsorption capacity of 4.39 mmol g<sup>-1</sup> at 0 °C and 1 atm was recently achieved using a microporous, nitrogen-doped porous carbon obtained by direct carbonization of an imidazolium-based IL containing nitrile groups, at 500 °C.<sup>32</sup> Notably, highly nitrogen-doped porous carbon materials obtained from low-cost, easily available, PILs/PSs are potential candidates for CO<sub>2</sub> capture.<sup>91</sup> In particular, [Dema][HSO<sub>4</sub>]-based carbon, despite its low surface area (690 m<sup>2</sup> g<sup>-1</sup>) and nitrogen content (2.1%), showed a higher CO<sub>2</sub> uptake (2.63 mmol g<sup>-1</sup> at 25 °C and 1 atm) than other carbons. Taking into account that both nitrogen content and microporous surface area are key issues for efficient CO<sub>2</sub> capture,<sup>187-190</sup> the remarkably high CO<sub>2</sub> uptake capacity is ascribed to its intensive and narrow pore size distribution of 1.12 nm, which is reported to be effective for efficient CO<sub>2</sub> adsorption.<sup>191-193</sup> In contrast, [Aan][HSO<sub>4</sub>]-based carbon, despite having the highest surface area (1380 m<sup>2</sup> g<sup>-1</sup>), showed the lowest CO<sub>2</sub> uptake, with a value of 1.63 mmol g<sup>-1</sup>; this is probably because of its large micropores and wide pore size distribution, which extends to mesopores and macropores.

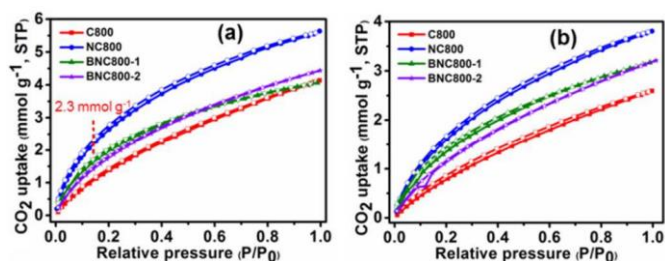


**Figure 36** CO<sub>2</sub> uptakes at (a) 273 K and (b) 298 K by N- and BN-decorated nanoporous carbons derived from IL and MOF. [Reproduced from Ref. 156.]

Nitrogen- and nitrogen/boron-doped nanoporous carbons with high nitrogen contents and large surface areas, obtained by cocarbonization of cyano-containing ILs and MOFs, exhibited excellent CO<sub>2</sub> adsorption capacities.<sup>156</sup> As shown in Figure 36a, sample NC800, obtained from [EMIm][DCA] at 800 °C, which has the highest basic nitrogen content (14.8 wt%), but a lower surface area (2397 m<sup>2</sup> g<sup>-1</sup>) than undecorated carbon C800 (2731 m<sup>2</sup> g<sup>-1</sup>), showed much higher CO<sub>2</sub> uptakes at 1 atm (5.7 mmol g<sup>-1</sup> at 273 K and 3.8 mmol g<sup>-1</sup> at 298 K) compared with C800 (4.1 mmol g<sup>-1</sup> at 273 K and 2.6 mmol g<sup>-1</sup> at 298 K). The high microporosity and high charge density at the nitrogen sites, which might facilitate interactions with polarizable acidic CO<sub>2</sub> molecules through local dipole–quadrupole interactions,<sup>187, 194</sup>

were predominantly responsible for the marked improvement in CO<sub>2</sub> uptake capacity. DES-based carbons are also potential candidates for efficient CO<sub>2</sub> capture, but in this case, nitrogen-containing components such as tetraethylammonium bromide or 3-hydroxypyridine are often needed for nitrogen doping into the final carbon to improve the CO<sub>2</sub> capacity.<sup>85-87</sup> Nitrogen-doped carbon monoliths with high microporous surface areas, obtained from a DES containing resorcinol, 3-hydroxypyridine, and tetraethylammonium bromide, are particularly suitable for CO<sub>2</sub> capture, and have outstanding adsorption capacities of up to 3.3 mmol g<sup>-1</sup> at 25 °C, along with excellent recyclabilities and stabilities.<sup>86</sup> It is known that the adsorption performance of CO<sub>2</sub> capture for N-doped porous carbon materials is generally evaluated by the adsorption capacity at 0 °C and 25 °C, adsorption heat, selectivity, etc. Table 5 summarized these values for ILs/DES-based carbons. Both ILs and DES-derived carbons exhibited moderate heats of adsorption for CO<sub>2</sub>, thus avoiding the energy penalties that are typically required for regeneration of functionalized adsorbents. In addition, ILs-derived carbons obviously exhibit a much higher selectivity than DES-derived carbons. Very interestingly, carbon monoliths with a tailor-made narrow microporosity obtained from specific DES (DES-7 and DES-8), despite their very low surface areas (ca. 4 m<sup>2</sup> g<sup>-1</sup>, determined by N<sub>2</sub> sorption at 77 K), exhibit good capacities, even comparable to the ILs-derived carbons with very high surface areas, as listed in Table 5. This unexpected result could be ascribed to the small micropore (ca. 0.6 nm) of the carbon material. As a molecular sieve network, such a narrow pore dimension restricted the diffusion of N<sub>2</sub> at 77 K, while selectively adsorbed CO<sub>2</sub> with a smaller molecular size.<sup>85</sup>

#### 6.5. Chemical catalysis

It is known that precious metals such as Pt coordinated within a highly nitrogen-rich environment are stable enough to survive several recycling steps.<sup>195</sup> Their combination of high nitrogen content and excellent porosity make IL-derived porous carbons promising candidates as catalyst supports for stabilizing highly dispersed precious-metal nanoparticles (e.g., Pd, Au, and Ru) for various applications such as biomass refining,<sup>146</sup> Ullmann coupling reactions,<sup>141, 148</sup> hydrogenation,<sup>111, 196</sup> aerobic oxidation,<sup>139</sup> carbonylation,<sup>121</sup> and phenylacetylene reduction.<sup>75, 150</sup>

The heterojunction between nitrogen-doped carbon and metal nanoparticles is believed to lead to very stable and uniform dispersion of metal nanoparticles and additional electronic activation of the metal nanoparticles, resulting in high catalytic performances. For example, a task-specific IL, [3BMP][DCA], as a precursor and colloidal silica as a hard template, accompanied by a post-deposition method, were used to form heterogeneous mesoporous nitrogen-doped carbon with a high nitrogen content (12 wt%) as a support for Pd nanoparticles.<sup>146</sup> The HRTEM images show that Pd nanoparticles of average size 4.1 nm were well dispersed on the surface of the nitrogen-doped carbon (Figure 37). Two Pd crystal planes, *i.e.*, (111) and (200) are clearly observed, with a plane angle of 55°. The resulting novel Pd catalyst shows very high catalytic activity in hydrodeoxygenation of vanillin (a typical model compound for lignin) at low hydrogen pressure under mild conditions, using water as a clean solvent. Excellent catalytic results (100% conversion of vanillin and 100% selectivity for 2-methoxy-4-methylphenol) were achieved without loss of catalytic activity after six cycles.

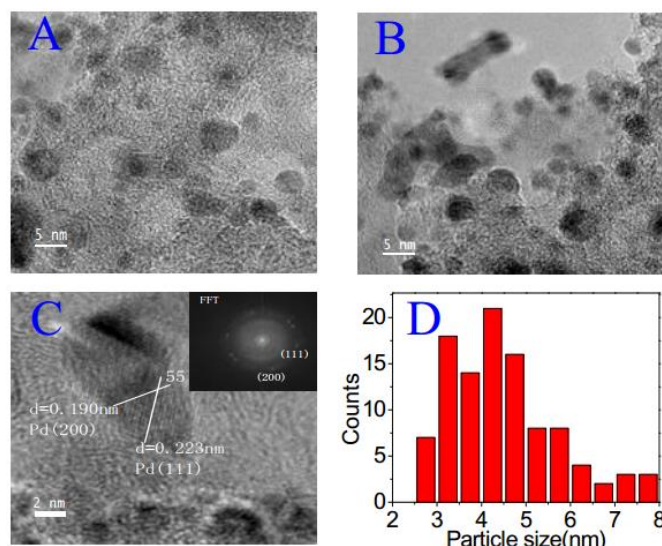


**Figure 37** HRTEM images and particle size distribution of Pd nanoparticles supported on IL-derived mesoporous nitrogen-doped carbon. [Reprinted with permission from Ref. 146, copyright 2012 American Chemical Society.]

Using ILs as precursors also provided us with a novel in situ method other than the wet chemical reduction method to prepare carbon supported precious-metal nanoparticles.<sup>139, 146</sup>

For example, precious-metal nanoparticles supported on porous carbon can be obtained by “one-pot” carbonization of metal-containing ILs,<sup>75, 111, 119, 121</sup> wherein ILs and metal salt behave as organic carbon precursor and metal source, respectively. In contrast to the traditional postdeposition and reduction method, the in situ one-step method may give rise to a more homogenous distribution of the metal nanoparticles. Most work stressed the important effect of high N content on catalysis for ILs-derived carbons, however, full understanding the real role of the doped N remains challenging. In addition, despite the significant advance in the catalytic application of ILs-derived carbons, most of the reported catalysts were limited to precious-metal nanoparticles, only very few works related to nonprecious metals.<sup>148</sup> It should be noted that in addition to behaving as a catalyst support to immobilize metal nanoparticles, N-doped carbon itself can also be directly used as a metal-free catalyst. In fact, this topic has attracted considerable attention in recent years.<sup>197-199</sup> Doping with heteroatoms makes it possible to control the physicochemical properties and therefore the catalytic performances of nanocarbons by introducing electron acceptors or donors.<sup>197</sup> For example, N-doped carbon materials were reported to be effective reusable catalysts for reactions such as Knoevenagel condensation<sup>198, 199</sup> and oxidative dehydrogenation.<sup>200</sup> In this respect, nitrogen-doped carbons obtained from IL precursors provide abundant active sites for catalysis. Shi *et al.* prepared carbon aerogels, using an IL as a soft template, and used them directly as catalysts in the selective oxidation of tetralin under mild conditions.<sup>108</sup> A typical carbon aerogel as a catalyst gave 30% conversion of tetralin to 1,2,3,4-tetrahydronaphthalen-1-ol and 3,4-dihydronaphthalen-1-one, with 78% selectivity. However, until now, little work has been done on the use of IL-based carbons as metal-free catalysts. Clearly, the investigation of IL-derived carbons in chemical catalysis is in its infancy. Further development of new catalytic applications and exploration of the correlation between carbon structure and catalytic activity are needed. For example, ILs-derived N-doped

porous carbon obtained at moderate temperatures with both high surface area and high nitrogen content may be potential solid base for base-catalyzed reactions.<sup>198, 199</sup> In fact, the abundant basic active sites possessed by such carbon materials have already been confirmed by their excellent ability for CO<sub>2</sub> adsorption.<sup>32, 174</sup>

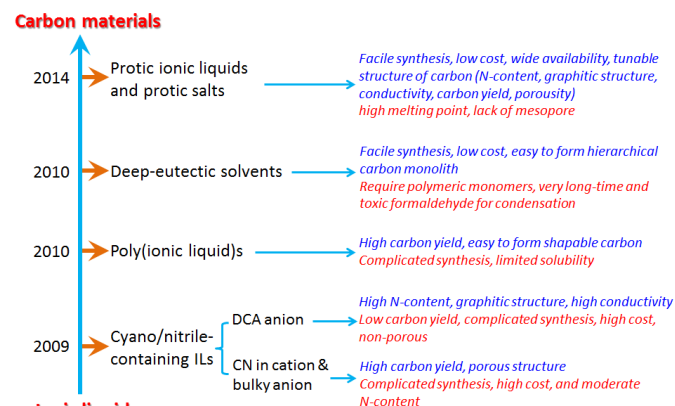


**Figure 38** Summary of recent developments of IL-based carbon precursors.

## 7. Conclusion and outlook

Successful carbonization of novel IL precursors represents a breakthrough in the fields of both ILs and carbon materials. This opens up a novel, direct, promising research direction for materialization of ILs, yielding carbons with distinct features for potential applications. We have reviewed the latest progress in the synthesis of carbon materials from ILs, which are alternative organic precursors that lead to a variety of carbonaceous materials. Carbon materials can be facilely obtained by direct carbonization of specific ILs at ambient pressure, without any complicated synthesis, catalyst, prepolymerization, vacuum system, or other complex techniques. The scope of IL-based carbonaceous precursors has been greatly expanded from the first cyano/nitrile-containing ILs to poly-ILs, DESs, and, more recently, PILs and PSs. As summarized in Figure 38, each of these possesses clear merits and disadvantages as carbon precursors. For general aprotic IL precursors, the key structural prerequisite is the presence of certain functional groups such as cyano/nitrile or vinyl groups that can undergo cross-linking reactions under pyrolysis conditions. For example, carbon materials derived from most [DCA]-based ILs have useful properties such as high nitrogen contents, developed graphitic structures, and high conductivities. However, the lower carbon yields, non-porous structures, and high costs of such ILs limit their use. The carbon yield can be improved by nanoconfinement and nanopores can be introduced using sophisticated nanocasting techniques. The high cost can be addressed by using them as dopants or surface-covering agents to reduce the amount of IL used. The poly-IL-based route is attractive, because carbons with morphologies such as tubes, fibers, membranes, monoliths, and spheres are easily obtained *via* different polymer-processing techniques. These shapeable carbon materials are expected to have applications in supported catalysis, as adsorbents, in gas separation, and in water treatment. However, complicated syntheses and additional polymerization of the IL monomers are required. DESs are cheap and can be easily synthesized, but they generally require special polymeric

monomers such as resorcinol, and long reaction times and toxic formaldehyde are necessary for condensation prior to carbonization. In contrast, PILs and PSs can be easily synthesized and are very low cost, as cheap as DESs, and are widely available. Importantly, depending on the precursor structure, the resultant carbons can be readily tuned to have a high specific surface area or high nitrogen content, high degree of graphitization, and high conductivity. However, nearly all porous carbons formed from PILs and PSs are microporous. The development of self-templated mesoporous carbons, as found in cyano/nitrile-containing ILs, is therefore highly desirable. It should be noted that non-carbonizable ILs can also be successfully transformed into carbon materials by nanoconfinement, energetic IL-template interactions, or simple microwave pyrolysis.

This review provides useful information on how to select and design suitable IL precursors for the preparation of task-specific carbon materials for “on-demand” applications. The large number of possible combinations of cations and anions provides a great opportunity for creating novel carbon materials with tailor-made structural morphologies, porosities, and surface areas from ILs. Moreover, when these novel precursors are used with established templating methods, advanced porous carbons with desirable porosities and the excellent intrinsic properties observed in IL-derived carbons can be fabricated, for high-performance applications in fields such as catalysis, gas capture and storage, electrochemistry, and energy.

Although this IL-based approach has proved to be extremely successful in the production of many distinctive carbon materials, the use of ILs for the synthesis of carbon materials is an emerging field and there are still many aspects to be studied and considered in the future.

- In-depth investigation of the correlation between precursor structure and final carbon material is required to modulate the properties of carbon nanomaterials by changing the chemical compositions of the precursors.
- Very few ILs containing both nitrile groups and bulky anions such as [NTf<sub>2</sub>] and [BETI] give mesoporous carbons *via* direct template-free carbonization, therefore further mechanistic analysis of mesopore formation is needed to enable rational design of specific IL precursors at the molecular level to obtain mesoporous structures.
- New IL precursors that may produce carbon with a simultaneously high surface area, high nitrogen content, and mesoporous structure *via* direct carbonization need to be developed. PILs and PSs are promising candidates, because of their low cost, easy synthesis, diverse structures, and wide availability.
- Functionalization of ILs to enable preparation of well-defined mesoporous carbon nanomaterials *via* combination with soft templates needs to be investigated.
- Advanced porous carbon materials need to be developed through rational combination of ILs and suitable templates. For example, it is possible to produce hierarchical porous carbon by combining ILs that can intrinsically yield micropores with macroscopic or mesoscopic silica templates.
- Expansion of the applications of IL-derived carbons is desirable.

All these further studies will extend the scope of this strategy and make it a really useful method that materials scientists will use on a regular basis to prepare carbon nanomaterials.

## Acknowledgements

This work was supported by the Japan Science and Technology Agency (JST) – Advanced Low Carbon Technology Research and Development Program (ALCA) of Japan.

## References

- J. P. Hallett and T. Welton, *Chem. Rev.*, 2011, **111**, 3508-3576.
- D. R. MacFarlane, N. Tachikawa, M. Forsyth, J. M. Pringle, P. C. Howlett, G. D. Elliott, J. H. Davis, M. Watanabe, P. Simon and C. A. Angell, *Energy Environ. Sci.*, 2014, **7**, 232-250.
- M. Smiglak, A. Metlen and R. D. Rogers, *Acc. Chem. Res.*, 2007, **40**, 1182-1192.
- T. Torimoto, T. Tsuda, K. Okazaki and S. Kuwabata, *Adv. Mater.*, 2010, **22**, 1196-1221.
- H. Xing, C. Liao, Q. Yang, G. M. Veith, B. Guo, X. G. Sun, Q. Ren, Y. S. Hu and S. Dai, *Angew. Chem. Int. Ed.*, 2014, **53**, 2099-2103.
- S.-Y. Lee, A. Ogawa, M. Kanno, H. Nakamoto, T. Yasuda and M. Watanabe, *J. Am. Chem. Soc.*, 2010, **132**, 9764-9773.
- E. Frackowiak, G. Lota and J. Pernak, *Appl. Phys. Lett.*, 2005, **86**, 164104.
- B. Mallick, B. Balke, C. Felser and A. V. Mudring, *Angew. Chem. Int. Ed.*, 2008, **47**, 7635-7638.
- T. Peppel, M. Köckerling, M. Geppert - Rybczyńska, R. V. Ralys, J. K. Lehmann, S. P. Verevkin and A. Heintz, *Angew. Chem. Int. Ed.*, 2010, **49**, 7116-7119.
- A. J. Boydston, C. S. Pecinovsky, S. T. Chao and C. W. Bielawski, *J. Am. Chem. Soc.*, 2007, **129**, 14550-14551.
- F. Zhou, Y. Liang and W. Liu, *Chem. Soc. Rev.*, 2009, **38**, 2590-2599.
- S. Schneider, T. Hawkins, M. Rosander, G. Vaghjiani, S. Chambreau and G. Drake, *Energy Fuels*, 2008, **22**, 2871-2872.
- R. Ryoo, S. H. Joo, M. Kruk and M. Jaroniec, *Adv. Mater.*, 2001, **13**, 677-681.
- C. D. Liang, Z. J. Li and S. Dai, *Angew. Chem. Int. Ed.*, 2008, **47**, 3696-3717.
- L. L. Zhang and X. Zhao, *Chem. Soc. Rev.*, 2009, **38**, 2520-2531.
- D. Jariwala, V. K. Sangwan, L. J. Lauhon, T. J. Marks and M. C. Hersam, *Chem. Soc. Rev.*, 2013, **42**, 2824-2860.
- M.-M. Titirici and M. Antonietti, *Chem. Soc. Rev.*, 2010, **39**, 103-116.
- T.-Y. Ma, L. Liu and Z.-Y. Yuan, *Chem. Soc. Rev.*, 2013, **42**, 3977-4003.
- A. Stein, S. G. Rudisill and N. D. Petkovich, *Chem. Mater.*, 2014, **26**, 259-276.
- Y. P. Zhai, Y. Wan, Y. Cheng, Y. F. Shi, F. Q. Zhang, B. Tu and D. Y. Zhao, *J. Porous Mater.*, 2008, **15**, 601-611.

- 21 J. P. Paraknowitsch and A. Thomas, *Macromol. Chem. Phys.*, 2012, **213**, 1132-1145.
- 22 T. P. Fellingner, A. Thomas, J. Yuan and M. Antonietti, *Adv. Mater.*, 2013, **25**, 5838-5855.
- 23 S. A. Forsyth, S. R. Batten, Q. Dai and D. R. MacFarlane, *Aust. J. Chem.*, 2004, **57**, 121-124.
- 24 T. J. Wooster, K. M. Johanson, K. J. Fraser, D. R. MacFarlane and J. L. Scott, *Green Chem.*, 2006, **8**, 691-696.
- 25 J. S. Lee, X. Q. Wang, H. M. Luo, G. A. Baker and S. Dai, *J. Am. Chem. Soc.*, 2009, **131**, 4596-4597.
- 26 J. P. Paraknowitsch, J. Zhang, D. S. Su, A. Thomas and M. Antonietti, *Adv. Mater.*, 2010, **22**, 87-92.
- 27 W. Yang, T. P. Fellingner and M. Antonietti, *J. Am. Chem. Soc.*, 2011, **133**, 206-209.
- 28 K. P. Gong, F. Du, Z. H. Xia, M. Durstock and L. M. Dai, *Science*, 2009, **323**, 760-764.
- 29 Y. Y. Shao, J. H. Sui, G. P. Yin and Y. Z. Gao, *Appl. Catal., B*, 2008, **79**, 89-99.
- 30 Y. Meng, D. Gu, F. Zhang, Y. Shi, H. Yang, Z. Li, C. Yu, B. Tu and D. Zhao, *Angew. Chem.*, 2005, **117**, 7215-7221.
- 31 J. S. Lee, X. Q. Wang, H. M. Luo and S. Dai, *Adv. Mater.*, 2010, **22**, 1004-1007.
- 32 X. Zhu, P. C. Hillesheim, S. M. Mahurin, C. M. Wang, C. C. Tian, S. Brown, H. M. Luo, G. M. Veith, K. S. Han, E. W. Hagaman, H. L. Liu and S. Dai, *ChemSusChem*, 2012, **5**, 1912-1917.
- 33 T.-P. Fellingner, D. S. Su, M. Engenhorst, D. Gautam, R. Schlögl and M. Antonietti, *J. Mater. Chem.*, 2012, **22**, 23996-24005.
- 34 J. P. Paraknowitsch, B. Wienert, Y. Zhang and A. Thomas, *Chem. Eur. J.*, 2012, **18**, 15416-15423.
- 35 J. P. Paraknowitsch, A. Thomas and M. Antonietti, *J. Mater. Chem.*, 2010, **20**, 6746-6758.
- 36 P. Kuhn, A. Forget, D. S. Su, A. Thomas and M. Antonietti, *J. Am. Chem. Soc.*, 2008, **130**, 13333-13337.
- 37 P. Kuhn, M. Antonietti and A. Thomas, *Angew. Chem. Int. Ed.*, 2008, **47**, 3450-3453.
- 38 E. Irran, B. Jürgens and W. Schnick, *Chem. Eur. J.*, 2001, **7**, 5372-5381.
- 39 J. S. Lee, H. Luo, G. A. Baker and S. Dai, *Chem. Mater.*, 2009, **21**, 4756-4758.
- 40 B. Guo, X. G. Sun, G. M. Veith, Z. Bi, S. M. Mahurin, C. Liao, C. Bridges, M. P. Paranthaman and S. Dai, *Adv. Energy Mater.*, 2013, **3**, 708-712.
- 41 P. F. Fulvio, J. S. Lee, R. T. Mayes, X. Wang, S. M. Mahurin and S. Dai, *Phys. Chem. Chem. Phys.*, 2011, **13**, 13486-13491.
- 42 N. Fechler, T.-P. Fellingner and M. Antonietti, *J. Mater. Chem. A*, 2013, **1**, 14097-14102.
- 43 X. Q. Wang and S. Dai, *Angew. Chem. Int. Ed.*, 2010, **49**, 6664-6668.
- 44 S. M. Chen, G. Z. Wu, M. L. Sha and S. R. Huang, *J. Am. Chem. Soc.*, 2007, **129**, 2416-2417.
- 45 J. Im, S. D. Cho, M. H. Kim, Y. M. Jung, H. S. Kim and H. S. Park, *Chem. Commun.*, 2012, **48**, 2015-2017.
- 46 M. Antonietti, D. Kuang, B. Smarsly and Y. Zhou, *Angew. Chem. Int. Ed.*, 2004, **43**, 4988-4992.
- 47 A. Chen, Y. Yu, H. Lv, Y. Wang, S. Shen, Y. Hu, B. Li, Y. Zhang and J. Zhang, *J. Mater. Chem. A*, 2013, **1**, 1045-1047.
- 48 Y. Ma, C. Zhang, G. Ji and J. Y. Lee, *J. Mater. Chem.*, 2012, **22**, 7845-7850.
- 49 S. Yoon, C. Liao, X.-G. Sun, C. A. Bridges, R. R. Unocic, J. Nanda, S. Dai and M. P. Paranthaman, *J. Mater. Chem.*, 2012, **22**, 4611-4614.
- 50 Z. Cui, S. Wang, Y. Zhang and M. Cao, *J. Power Sources*, 2014, **259**, 138-144.
- 51 X. Zhang, N. Böckenfeld, F. Berkemeier and A. Balducci, *ChemSusChem*, 2014, **7**, 1710-1718.
- 52 H. Song, N. Li, H. Cui and C. Wang, *Nano Energy*, 2014, **4**, 81-87.
- 53 Z. Ding, L. Zhao, L. Suo, Y. Jiao, S. Meng, Y.-S. Hu, Z. Wang and L. Chen, *Phys. Chem. Chem. Phys.*, 2011, **13**, 15127-15133.
- 54 A. Safavi, F. Sedaghati, H. Shahbaazi and E. Farjami, *RSC Adv.*, 2012, **2**, 7367-7370.
- 55 D. Xiao, D. Yuan, H. He and M. Gao, *J. Lumin.*, 2013, **140**, 120-125.
- 56 A. Zhao, C. Zhao, M. Li, J. Ren and X. Qu, *Anal. Chim. Acta*, 2014, **809**, 128-133.
- 57 N. E. Leadbeater and H. M. Torenius, *J. Org. Chem.*, 2002, **67**, 3145-3148.
- 58 J. Yuan and M. Antonietti, *Polymer*, 2011, **52**, 1469-1482.
- 59 J. Yuan, D. Mecerreyes and M. Antonietti, *Prog. Polym. Sci.*, 2013, **38**, 1009-1036.
- 60 J. Lu, F. Yan and J. Texter, *Prog. Polym. Sci.*, 2009, **34**, 431-448.
- 61 O. Green, S. Grubjesic, S. Lee and M. A. Firestone, *J. Macromol. Sci., Polym. Rev.*, 2009, **49**, 339-360.
- 62 J. Yuan, A. G. Márquez, J. Reinacher, C. Giordano, J. Janek and M. Antonietti, *Polymer Chemistry*, 2011, **2**, 1654-1657.
- 63 Y. Men, M. Siebenbürger, X. Qiu, M. Antonietti and J. Yuan, *J. Mater. Chem. A*, 2013, **1**, 11887-11893.
- 64 J. Balach, H. Wu, F. Polzer, H. Kirmse, Q. Zhao, Z. Wei and J. Yuan, *RSC Adv.*, 2013, **3**, 7979-7986.
- 65 D. Kuzmicz, P. Coupillaud, Y. Men, J. Vignolle, G. Vendraminetto, M. Ambroggi, D. Taton and J. Yuan, *Polymer*, 2014, **55**, 3423-3430.
- 66 Q. Zhao, T. P. Fellingner, M. Antonietti and J. Yuan, *Macromol. Rapid Commun.*, 2012, **33**, 1149-1153.
- 67 X. Bo, J. Bai, J. Ju and L. Guo, *J. Power Sources*, 2011, **196**, 8360-8365.
- 68 B. Wu, Y. Kuang, Y. Zhang, X. Zhang and J. Chen, *J. Mater. Chem.*, 2012, **22**, 13085-13090.

- 69 J. Yuan, C. Giordano and M. Antonietti, *Chem. Mater.*, 2010, **22**, 5003-5012.
- 70 J.-H. Jeon, K. Tanaka and Y. Chujo, *J. Mater. Chem. A*, 2014, **2**, 624-630.
- 71 F. Zheng, G. Mu, Z. Zhang, Y. Shen, M. Zhao and G. Pang, *Mater. Lett.*, 2012, **68**, 453-456.
- 72 S. Soll, T. P. Fellingner, X. Wang, Q. Zhao, M. Antonietti and J. Yuan, *Small*, 2013, **9**, 4135-4141.
- 73 J. Yuan, S. Soll, M. Drechsler, A. H. Müller and M. Antonietti, *J. Am. Chem. Soc.*, 2011, **133**, 17556-17559.
- 74 J. Yuan and M. Antonietti, *Macromolecules*, 2011, **44**, 744-750.
- 75 P. Zhang, J. Yuan, T. P. Fellingner, M. Antonietti, H. Li and Y. Wang, *Angew. Chem. Int. Ed.*, 2013, **52**, 6028-6032.
- 76 D. Carriazo, M. C. Serrano, M. C. Gutiérrez, M. L. Ferrer and F. del Monte, *Chem. Soc. Rev.*, 2012, **41**, 4996-5014.
- 77 Q. Zhang, K. D. O. Vigier, S. Royer and F. Jérôme, *Chem. Soc. Rev.*, 2012, **41**, 7108-7146.
- 78 A. P. Abbott, J. C. Barron, K. S. Ryder and D. Wilson, *Chem. Eur. J.*, 2007, **13**, 6495-6501.
- 79 A. P. Abbott, G. Capper, D. L. Davies, R. K. Rasheed and V. Tambyrajah, *Chem. Commun.*, 2003, 70-71.
- 80 E. R. Parnham, E. A. Drylie, P. S. Wheatley, A. M. Slawin and R. E. Morris, *Angew. Chem.*, 2006, **118**, 5084-5088.
- 81 D. V. Wagle, H. Zhao and G. A. Baker, *Acc. Chem. Res.*, 2014, **47**, 2299-2308.
- 82 M. a. C. Gutiérrez, F. Rubio and F. del Monte, *Chem. Mater.*, 2010, **22**, 2711-2719.
- 83 D. Carriazo, M. a. C. Gutiérrez, M. L. Ferrer and F. del Monte, *Chem. Mater.*, 2010, **22**, 6146-6152.
- 84 D. Carriazo, M. C. Gutiérrez, F. Picó, J. M. Rojo, J. L. Fierro, M. L. Ferrer and F. del Monte, *ChemSusChem*, 2012, **5**, 1405-1409.
- 85 J. Patiño, M. C. Gutiérrez, D. Carriazo, C. O. Ania, J. B. Parra, M. L. Ferrer and F. del Monte, *Energy Environ. Sci.*, 2012, **5**, 8699-8707.
- 86 M. C. Gutiérrez, D. Carriazo, C. O. Ania, J. B. Parra, M. L. Ferrer and F. del Monte, *Energy Environ. Sci.*, 2011, **4**, 3535-3544.
- 87 J. Patiño, M. Gutiérrez, D. Carriazo, C. Ania, J. Fierro, M. Ferrer and F. del Monte, *J. Mater. Chem. A*, 2014, **2**, 8719-8729.
- 88 D. Carriazo, M. C. Gutiérrez, R. Jiménez, M. L. Ferrer and F. del Monte, *Part. Part. Syst. Char.*, 2013, **30**, 316-320.
- 89 M. C. Gutiérrez, D. Carriazo, A. Tamayo, R. Jiménez, F. Picó, J. M. Rojo, M. L. Ferrer and F. del Monte, *Chem. Eur. J.*, 2011, **17**, 10533-10537.
- 90 N. López-Salas, M. C. Gutiérrez, C. O. Ania, J. L. G. Fierro, M. L. Ferrer and F. del Monte, *J. Mater. Chem. A*, 2014, **2**, 17387-17399.
- 91 S. Zhang, K. Dokko and M. Watanabe, *Chem. Mater.*, 2014, **26**, 2915-2926.
- 92 M. S. Miran, H. Kinoshita, T. Yasuda, M. A. Susan and M. Watanabe, *Phys. Chem. Chem. Phys.*, 2012, **14**, 5178-5186.
- 93 S. Zhang, M. S. Miran, A. Ikoma, K. Dokko and M. Watanabe, *J. Am. Chem. Soc.*, 2014, **136**, 1690-1693.
- 94 Y. Gogotsi, A. Nikitin, H. H. Ye, W. Zhou, J. E. Fischer, B. Yi, H. C. Foley and M. W. Barsoum, *Nat. Mater.*, 2003, **2**, 591-594.
- 95 W. Ding, Z. Wei, S. Chen, X. Qi, T. Yang, J. Hu, D. Wang, L.-J. Wan, S. F. Alvi and L. Li, *Angew. Chem. Int. Ed.*, 2013, **52**, 11755-11759.
- 96 R. Czerw, M. Terrones, J. C. Charlier, X. Blase, B. Foley, R. Kamalakaran, N. Grobert, H. Terrones, D. Tekleab, P. M. Ajayan, W. Blau, M. Ruhle and D. L. Carroll, *Nano Lett.*, 2001, **1**, 457-460.
- 97 J. D. Wiggins-Camacho and K. J. Stevenson, *J. Phys. Chem. C*, 2009, **113**, 19082-19090.
- 98 L. Zhao, Y. S. Hu, H. Li, Z. X. Wang and L. Q. Chen, *Adv. Mater.*, 2011, **23**, 1385-1388.
- 99 J. Cao, Y. Chu and X. Tan, *Mater. Chem. Phys.*, 2014, **144**, 17-24.
- 100 J. PeteráParaknowitsch, *Phys. Chem. Chem. Phys.*, 2012, **14**, 6444-6447.
- 101 Z. Y. Jin, A. H. Lu, Y. Y. Xu, J. T. Zhang and W. C. Li, *Adv. Mater.*, 2014, **26**, 3700-3705.
- 102 Y. Yan, Y.-X. Yin, S. Xin, Y.-G. Guo and L.-J. Wan, *Chem. Commun.*, 2012, **48**, 10663-10665.
- 103 M. Zhou, X. Li, J. Cui, T. Liu, T. Cai, H. Zhang and S. Guan, *Int. J. Electrochem. Sci.*, 2012, **7**, 9984-9996.
- 104 Q. DucáTruong, *J. Mater. Chem. C*, 2013, **1**, 1713-1716.
- 105 D.-C. Guo, J. Mi, G.-P. Hao, W. Dong, G. Xiong, W.-C. Li and A.-H. Lu, *Energy Environ. Sci.*, 2013, **6**, 652-659.
- 106 Y. Wang, J. Zhang, X. Wang, M. Antonietti and H. Li, *Angew. Chem. Int. Ed.*, 2010, **49**, 3356-3359.
- 107 G. Wang, Z. Ling, C. Li, Q. Dong, B. Qian and J. Qiu, *Electrochem. Commun.*, 2013, **31**, 31-34.
- 108 H. Yang, X. Cui, Y. Deng and F. Shi, *J. Mater. Chem.*, 2012, **22**, 21852-21856.
- 109 H. Byun, G. Nam, Y. Rhym and S. Shim, *Carbon Lett*, 2012, **13**, 94-98.
- 110 J. S. Lee, R. T. Mayes, H. Luo and S. Dai, *Carbon*, 2010, **48**, 3364-3368.
- 111 X. Cui, F. Shi and Y. Deng, *ChemCatChem*, 2012, **4**, 333-336.
- 112 Y. Yao, T. Zhou, T. Yang, R. Xiang and Y. Wu, *Carbon*, 2013, **58**, 249-251.
- 113 Z.-L. Xie, R. J. White, J. Weber, A. Taubert and M. M. Titirici, *J. Mater. Chem.*, 2011, **21**, 7434-7442.
- 114 P. FernandoáFulvio, P. ChristopheráHillesheim, J. ChristopheráBauer and S. MarkáMahurin, *J. Mater. Chem. A*, 2013, **1**, 59-62.

- 115 J. H. Hafner, M. J. Bronikowski, B. R. Azamian, P. Nikolaev, A. G. Rinzler, D. T. Colbert, K. A. Smith and R. E. Smalley, *Chem. Phys. Lett.*, 1998, **296**, 195-202.
- 116 T. Kyotani, *Carbon*, 2000, **38**, 269-286.
- 117 R. Göbel, Z.-L. Xie, M. Neumann, C. Günter, R. Löbbecke, S. Kubo, M.-M. Titirici, C. Giordano and A. Taubert, *CrystEngComm*, 2012, **14**, 4946-4951.
- 118 K. H. Lim and H. Kim, *Appl. Catal., B*, 2014, **158**, 355-360.
- 119 C. Pan, L. Qiu, Y. Peng and F. Yan, *J. Mater. Chem.*, 2012, **22**, 13578-13584.
- 120 Y. Peng, X. Wu, L. Qiu, C. Liu, S. Wang and F. Yan, *J. Mater. Chem. A*, 2013, **1**, 9257-9263.
- 121 Z. Li, J. Liu, Z. Huang, Y. Yang, C. Xia and F. Li, *ACS Catal.*, 2013, **3**, 839-845.
- 122 J. Yuan, H. Schlaad, C. Giordano and M. Antonietti, *Eur. Polym. J.*, 2011, **47**, 772-781.
- 123 N. Fechler, T.-P. Fellingner and M. Antonietti, *Chem. Mater.*, 2012, **24**, 713-719.
- 124 N. Fechler, G. A. Tiruye, R. MARCILLA and M. Antonietti, *RSC Adv.*, 2014, **4**, 26981-26989.
- 125 M. Kruk and M. Jaroniec, *Chem. Mater.*, 2001, **13**, 3169-3183.
- 126 Q. Zhao, T.-P. Fellingner, M. Antonietti and J. Yuan, *J. Mater. Chem. A*, 2013, **1**, 5113-5120.
- 127 P. F. Fulvio, P. C. Hillesheim, Y. Oyola, S. M. Mahurin, G. M. Veith and S. Dai, *Chem. Commun.*, 2013, **49**, 7289-7291.
- 128 Z. Zhang, G. M. Veith, G. M. Brown, P. F. Fulvio, P. C. Hillesheim, S. Dai and S. H. Overbury, *Chem. Commun.*, 2014, **50**, 1469-1471.
- 129 S. Jun, S. H. Joo, R. Ryoo, M. Kruk, M. Jaroniec, Z. Liu, T. Ohsuna and O. Terasaki, *J. Am. Chem. Soc.*, 2000, **122**, 10712-10713.
- 130 A. J. Zarbin, R. Bertholdo and M. A. Oliveira, *Carbon*, 2002, **40**, 2413-2422.
- 131 S. Tabata, Y. Isshiki and M. Watanabe, *J. Electrochem. Soc.*, 2008, **155**, K42-K49.
- 132 A. Lu, A. Kiefer, W. Schmidt and F. Schüth, *Chem. Mater.*, 2004, **16**, 100-103.
- 133 Z. Ma, J. Yu and S. Dai, *Adv. Mater.*, 2010, **22**, 261-285.
- 134 Y. Zhou and M. Antonietti, *J. Am. Chem. Soc.*, 2003, **125**, 14960-14961.
- 135 T. Nakashima and N. Kimizuka, *J. Am. Chem. Soc.*, 2003, **125**, 6386-6387.
- 136 Y. Zhou, J. H. Schattka and M. Antonietti, *Nano Lett.*, 2004, **4**, 477-481.
- 137 D. Zhang, T. Yan, H. Li and L. Shi, *Microporous Mesoporous Mater.*, 2011, **141**, 110-118.
- 138 B. Karimi, H. Behzadnia, M. Rafiee and H. Vali, *Chem. Commun.*, 2012, **48**, 2776-2778.
- 139 B. Karimi, H. Behzadnia, M. Bostina and H. Vali, *Chem. Eur. J.*, 2012, **18**, 8634-8640.
- 140 S. H. Kazemi, B. Karimi, A. Fashi, H. Behzadnia and H. Vali, *J. Solid State Electrochem.*, 2014, 1-6.
- 141 B. Karimi, H. Behzadnia and H. Vali, *ChemCatChem*, 2014, **6**, 745-748.
- 142 B. Qiu, C. Pan, W. Qian, Y. Peng, L. Qiu and F. Yan, *J. Mater. Chem. A*, 2013, **1**, 6373-6378.
- 143 D. Zhao, J. Feng, Q. Huo, N. Melosh, G. H. Fredrickson, B. F. Chmelka and G. D. Stucky, *science*, 1998, **279**, 548-552.
- 144 D. Zhao, Q. Huo, J. Feng, B. F. Chmelka and G. D. Stucky, *J. Am. Chem. Soc.*, 1998, **120**, 6024-6036.
- 145 T. P. Fellingner, F. Hasche, P. Strasser and M. Antonietti, *J. Am. Chem. Soc.*, 2012, **134**, 4072-4075.
- 146 X. Xu, Y. Li, Y. T. Gong, P. F. Zhang, H. R. Li and Y. Wang, *J. Am. Chem. Soc.*, 2012, **134**, 16987-16990.
- 147 F. Hasché, T. P. Fellingner, M. Oezaslan, J. P. Paraknowitsch, M. Antonietti and P. Strasser, *ChemCatChem*, 2012, **4**, 479-483.
- 148 P. Zhang, J. Yuan, H. Li, X. Liu, X. Xu, M. Antonietti and Y. Wang, *RSC Adv.*, 2013, **3**, 1890-1895.
- 149 J. P. Paraknowitsch, Y. Zhang and A. Thomas, *J. Mater. Chem.*, 2011, **21**, 15537-15543.
- 150 C. Liu, P. Tang, A. Chen, Y. Hu, Y. Yu, H. Lv and D. Ma, *Mater. Lett.*, 2013, **108**, 285-288.
- 151 N. Fechler, T. P. Fellingner and M. Antonietti, *Adv. Mater.*, 2013, **25**, 75-79.
- 152 X. Liu, N. Fechler and M. Antonietti, *Chem. Soc. Rev.*, 2013, **42**, 8237-8265.
- 153 X. Liu and M. Antonietti, *Carbon*, 2014, **69**, 460-466.
- 154 M. Antonietti, K. Elumeeva, N. Fechler and T. Fellingner, *Mater. Horiz.*, 2014, **1**, 588-594.
- 155 B. Liu, H. Shioyama, T. Akita and Q. Xu, *J. Am. Chem. Soc.*, 2008, **130**, 5390-5391.
- 156 A. Aijaz, T. Akita, H. Yang and Q. Xu, *Chem. Commun.*, 2014, **50**, 6498-6501.
- 157 J. P. Paraknowitsch, Y. Zhang, B. Wienert and A. Thomas, *Chem. Commun.*, 2013, **49**, 1208-1210.
- 158 A. M. Puziy, O. I. Poddubnaya, A. Martinez-Alonso, F. Suarez-Garcia and J. M. D. Tascon, *Carbon*, 2003, **41**, 1181-1191.
- 159 A. M. Puziy, O. I. Poddubnaya, A. Martinez-Alonso, F. Suarez-Garcia and J. M. D. Tascon, *Carbon*, 2002, **40**, 1493-1505.
- 160 A. M. Puziy, O. I. Poddubnaya, A. Martinez-Alonso, F. Suarez-Garcia and J. M. D. Tascon, *Carbon*, 2002, **40**, 1507-1519.
- 161 Y. J. Wang, D. P. Wilkinson and J. J. Zhang, *Chem. Rev.*, 2011, **111**, 7625-7651.
- 162 Z. Chen, M. Waje, W. Li and Y. Yan, *Angew. Chem. Int. Ed.*, 2007, **46**, 4060-4063.
- 163 H.-W. Liang, W. Wei, Z.-S. Wu, X. Feng and K. Müllen, *J. Am. Chem. Soc.*, 2013, **135**, 16002-16005.

- 164 Y. H. Bing, H. S. Liu, L. Zhang, D. Ghosh and J. J. Zhang, *Chem. Soc. Rev.*, 2010, **39**, 2184-2202.
- 165 N.-D. O. M. G. Arrays, *Angew. Chem. Int. Ed.*, 2010, **49**, 2565-2569.
- 166 K. Q. Jian, H. S. Shim, A. Schwartzman, G. P. Crawford and R. H. Hurt, *Adv. Mater.*, 2003, **15**, 164-167.
- 167 C. Han, J. Wang, Y. Gong, X. Xu, H. Li and Y. Wang, *J. Mater. Chem. A*, 2014, **2**, 605-609.
- 168 N. Ranjbar Sahraie, J. P. Paraknowitsch, C. Goebel, A. Thomas and P. Strasser, *J. Am. Chem. Soc.*, 2014, **136**, 14486-14497.
- 169 J. Liang, Y. Jiao, M. Jaroniec and S. Z. Qiao, *Angew. Chem. Int. Ed.*, 2012, **51**, 11496-11500.
- 170 N. A. Kaskhedikar and J. Maier, *Adv. Mater.*, 2009, **21**, 2664-2680.
- 171 S. Yang, X. Feng, L. Zhi, Q. Cao, J. Maier and K. Müllen, *Adv. Mater.*, 2010, **22**, 838-842.
- 172 M.-H. Ryu, K.-N. Jung, K.-H. Shin, K.-S. Han and S. Yoon, *J. Phys. Chem. C*, 2013, **117**, 8092-8098.
- 173 Y. Ni, Y. Yin, P. Wu, H. Zhang and C. Cai, *ACS Appl. Mater. Inter.*, 2014, **6**, 7346-7355.
- 174 S. M. Mahurin, P. F. Fulvio, P. C. Hillesheim, K. M. Nelson, G. M. Veith and S. Dai, *ChemSusChem*, 2014, DOI: 10.1002/cssc.201402338.
- 175 L. Qie, W. M. Chen, Z. H. Wang, Q. G. Shao, X. Li, L. X. Yuan, X. L. Hu, W. X. Zhang and Y. H. Huang, *Adv. Mater.*, 2012, **24**, 2047-2050.
- 176 A. S. Aricò, P. Bruce, B. Scrosati, J.-M. Tarascon and W. Van Schalkwijk, *Nat. Mater.*, 2005, **4**, 366-377.
- 177 D. Hulicova-Jurcakova, A. M. Puziy, O. I. Poddubnaya, F. Suárez-García, J. M. Tascón and G. Q. Lu, *J. Am. Chem. Soc.*, 2009, **131**, 5026-5027.
- 178 L.-F. Chen, X.-D. Zhang, H.-W. Liang, M. Kong, Q.-F. Guan, P. Chen, Z.-Y. Wu and S.-H. Yu, *ACS Nano*, 2012, **6**, 7092-7102.
- 179 L. Zhao, L. Z. Fan, M. Q. Zhou, H. Guan, S. Qiao, M. Antonietti and M. M. Titirici, *Adv. Mater.*, 2010, **22**, 5202-5206.
- 180 R. Mysyk, E. Raymundo-Piñero, M. Anouti, D. Lemordant and F. Béguin, *Electrochem. Commun.*, 2010, **12**, 414-417.
- 181 K. M. K. Yu, I. Curcic, J. Gabriel and S. C. E. Tsang, *Chemsuschem*, 2008, **1**, 893-899.
- 182 D. M. D'Alessandro, B. Smit and J. R. Long, *Angew. Chem. Int. Ed.*, 2010, **49**, 6058-6082.
- 183 A.-H. Lu and G.-P. Hao, *Annu. Rep. Prog. Chem., Sect. A: Inorg. Chem.*, 2013, **109**, 484-503.
- 184 G. P. Hao, W. C. Li, D. Qian, G. H. Wang, W. P. Zhang, T. Zhang, A. Q. Wang, F. Schuth, H. J. Bongard and A. H. Lu, *J. Am. Chem. Soc.*, 2011, **133**, 11378-11388.
- 185 G. P. Hao, W. C. Li, D. Qian and A. H. Lu, *Adv. Mater.*, 2010, **22**, 853-857.
- 186 X. Zhu, C. Tian, S. Chai, K. Nelson, K. S. Han, E. W. Hagaman, G. M. Veith, S. M. Mahurin, H. Liu and S. Dai, *Adv. Mater.*, 2013, **25**, 4152-4158.
- 187 M. Sevilla, P. Valle-Vigón and A. B. Fuertes, *Adv. Funct. Mater.*, 2011, **21**, 2781-2787.
- 188 V. Chandra, S. U. Yu, S. H. Kim, Y. S. Yoon, D. Y. Kim, A. H. Kwon, M. Meyyappan and K. S. Kim, *Chem. Commun.*, 2012, **48**, 735-737.
- 189 W. Xing, C. Liu, Z. Y. Zhou, L. Zhang, J. Zhou, S. P. Zhuo, Z. F. Yan, H. Gao, G. Q. Wang and S. Z. Qiao, *Energy Environ. Sci.*, 2012, **5**, 7323-7327.
- 190 M. Nandi, K. Okada, A. Dutta, A. Bhaumik, J. Maruyama, D. Derks and H. Uyama, *Chem. Commun.*, 2012, **48**, 10283-10285.
- 191 A. Vishnyakov, P. I. Ravikovitch and A. V. Neimark, *Langmuir*, 1999, **15**, 8736-8742.
- 192 J. M. Martinmartinez, R. Torregrosamacia and M. C. Mittelmeijerhazeleger, *Fuel*, 1995, **74**, 111-114.
- 193 D. CazorlaAmoros, J. AlcanizMonge and A. LinaresSolano, *Langmuir*, 1996, **12**, 2820-2824.
- 194 H. Choi, Y. C. Park, Y.-H. Kim and Y. S. Lee, *J. Am. Chem. Soc.*, 2011, **133**, 2084-2087.
- 195 R. Palkovits, M. Antonietti, P. Kuhn, A. Thomas and F. Schüth, *Angew. Chem. Int. Ed.*, 2009, **48**, 6909-6912.
- 196 X. Xu, H. Li and Y. Wang, *ChemCatChem*, 2014, DOI:10.1002/cctc.201402561R1.
- 197 D. S. Su, S. Perathoner and G. Centi, *Chem. Rev.*, 2013, **113**, 5782-5816.
- 198 S. Dommele and K. P. áde Jong, *Chem. Commun.*, 2006, 4859-4861.
- 199 N. Kan - nari, S. Okamura, S. i. Fujita, J. i. Ozaki and M. Arai, *Adv. Synth. Catal.*, 2010, **352**, 1476-1484.
- 200 J. Zhang, X. Liu, R. Blume, A. Zhang, R. Schlögl and D. S. Su, *Science*, 2008, **322**, 73-77.